2017-06

Settling-driven gravitational instabilities associated with volcanic clouds: new insights from experimental investigations

Scollo, S

10.1007/s00445-017-1124-x
Bulletin of Volcanology
Springer Science and Business Media LLC

Bulletin of Volcanology

Settling-driven gravitational instabilities associated with volcanic clouds: new insights from experimental investigations

--Manuscript Draft--

Manuscript Number:	BUVO-D-16-00052R3
Full Title:	Settling-driven gravitational instabilities associated with volcanic clouds: new insights from experimental investigations
Article Type:	Research Article
Corresponding Author:	Simona Scollo, PhD Istituto Nazionale di Geofisica e Vulcanologia, Osservatorio Etneo 95123, ITALY
Corresponding Author Secondary Information:	
Order of Authors:	Simona Scollo, PhD
	Costanza Bonadonna
	Irene Manzella
Funding Information:	ESF Research Networking Programmes (Reference N°4257 MeMoVolc) — Dr Simona Scollo
	Swiss National Science Foundation (No 200021_156255) — Prof Costanza Bonadonna
Abstract:	Downward propagating instabilities are often observed at the bottom of volcanic plumes and clouds. These instabilities generate fingers that enhance the sedimentation of fine ash. Despite their potential influence on tephra dispersal and deposition, their dynamics is not entirely understood, undermining the accuracy of volcanic ash transport and dispersal models. Here, we present new laboratory experiments that investigate the effects of particle size, composition and concentration on finger generation and dynamics. The experimental set-up consists of a Plexiglas tank equipped with a removable plastic sheet that separates two different layers. The lower layer is a solution of water and sugar, initially denser than the upper layer, which consists of water and particles. Particles in the experiments include glass beads as well as andesitic, rhyolitic, and basaltic volcanic ash. During the experiments, we removed the horizontal plastic sheet separating the two fluids. Particles were illuminated with a laser and filmed with a HD camera; the Particle Image Velocimetry (PIV) is used to analyse finger dynamics. Results show that both the number and the downward advance speed of fingers increase with particle concentration in the upper layer, while finger speed increases with particle size but is independent of particle composition. An increase in particle concentration and turbulence is estimated to take place inside the fingers, which could promote aggregation in subaerial fallout events. Finally, finger number, finger speed and particle concentration were observed to decrease with time after the formation of fingers. A similar pattern could occur in volcanic clouds when the mass supply from the eruptive vent is reduced. Observed evolution of the experiments through time also indicates that there must be a threshold of fine ash concentration and mass eruption rate below which fingers do not form; this is also confirmed by field observations.
Response to Reviewers:	Dear Executive Editor, We have accepted all your suggestions indicated on your annotated paper and made the final changes indicated on your annotated paper. Thanking for your co-operation, Best Regards, Simona Scollo, On the behalf of all authors

Settling-driven gravitational instabilities associated with volcanic clouds: new insights from experimental investigations

Simona Scollo[1], Costanza Bonadonna[2], Irene Manzella[2]

Istituto Nazionale di Geofisica e Vulcanologia, Osservatorio Etneo, Sezione di Catania, Italy

Département des sciences de la Terre, Université de Genève, Suisse

Abstract

Downward propagating instabilities are often observed at the bottom of volcanic plumes and clouds. These instabilities generate fingers that enhance the sedimentation of fine ash. Despite their potential influence on tephra dispersal and deposition, their dynamics is not entirely understood, undermining the accuracy of volcanic ash transport and dispersal models. Here, we present new laboratory experiments that investigate the effects of particle size, composition and concentration on finger generation and dynamics. The experimental set-up consists of a Plexiglas tank equipped with a removable plastic sheet that separates two different layers. The lower layer is a solution of water and sugar, initially denser than the upper layer, which consists of water and particles. Particles in the experiments include glass beads as well as andesitic, rhyolitic, and basaltic volcanic ash. During the experiments, we removed the horizontal plastic sheet separating the two fluids. Particles were illuminated with a laser and filmed with a HD camera; the Particle Image Velocimetry (PIV) is used to analyse finger dynamics. Results show that both the number and the downward advance speed of fingers increase with particle concentration in the upper layer, while finger speed increases with particle size but is independent of particle composition. An increase in particle concentration and turbulence is estimated to take place inside the fingers, which could promote aggregation in subaerial fallout events. Finally, finger number, finger speed and particle concentration were observed to decrease with time after the formation of fingers. A similar pattern

could occur in volcanic clouds when the mass supply from the eruptive vent is reduced. Observed evolution of the experiments through time also indicates that there must be a threshold of fine ash concentration and mass eruption rate below which fingers do not form; this is also confirmed by field observations.

Key words: Tephra; Volcanic Plumes; Volcanic Ash; Laboratory Experiments; PIV Analysis; Particle Aggregation.

1. INTRODUCTION

During explosive volcanic eruptions, a large number of volcanic particles is injected into the atmosphere with the potential of generating significant hazards to nearby communities and various economic sectors. While fine ash in distal area may produce long-term health risks and is extremely dangerous for aircraft jet engines due to the accumulation of melted glass particles and erosion of turbine blades, proximal fallout can cause collapse of buildings and damage to agriculture, vegetation, lifelines, road networks and critical infrastructures (e.g. Blong, 2000; Miller and Casadevall, 2000). The volcanic crisis of Eyafjallajökull volcano (2010, Iceland) and Cordón Caulle volcano (2011, Chile), represent the most recent examples of widespread economic disruption caused by volcanic ash (e.g. Alexander, 2013; Oxford, 2010; Elissondo et al., 2016; Sammons et al., 2010; Wilson et al., 2013). Volcanic risk can be mitigated thanks to accurate forecasting of tephra dispersal that builds on a good understanding and description of volcanic plumes and cloud dynamics and sedimentation. There is a variety of volcanic ash dispersal models based on different assumptions and modelling strategies (see Folch et al. (2012) for a review). Sensitivity analyses have demonstrated that, when eruption source parameters are well constrained, eruptive phenomena such as particle dispersal and sedimentation can be reproduced with good accuracy (e.g. Costa et al., 2006; Scollo et al., 2010; Bonadonna et al., 2012). However, even after an accurate model calibration, differences between field data and model results can reach up to 150% (e.g. Scollo et al., 2008). Causes of these discrepancies include the fact that not all the physical processes of volcanic plumes and clouds are fully described. Among these processes, the generation and dynamics of fingers associated with settling-driven gravitational instabilities, also called convective instabilities, could play an important role (e.g. Carazzo and Jellinek, 2013; Durant, 2015; Manzella et al., 2015; Figure 1).

In the presence of particle-laden fluids, such as volcanic plumes and clouds, gravitational instabilities are induced by particle settling across the density interface (Hoyal et al., 1999). Initially the configuration is gravitationally stable: the lighter particle laden fluid (e.g. volcanic

current) is emplaced above the denser one (e.g. atmospheric layer). Small variations in density at different points of the interface occur due to particle settling, generating instabilities. As a consequence, vertical gravity currents, called fingers, start to develop in the lower layer and lead to convective motion (Turner, 1979), which drives the vertical transport of particles in the lower layer (e.g. Carazzo and Jellinek, 2012; Hoyal et al., 1999; Manzella et al., 2015). The main condition for the formation of settling-driven gravitational instabilities is that the particle suspension behaves as a continuum and this happens if the finger downward velocity has to be greater than particle settling velocity (Hoyal et al., 1999). This condition (e.g. the particles to be coupled with the fluid and efficiently mixed) is satisfied, according to Carazzo and Jellinek (2012), when both the Stokes number ($St = \frac{1}{f}\frac{\rho_p}{18}\frac{d_p^2}{\mu}\frac{V}{L}$) and the Sedimentation number ($\sum = \frac{1}{f}\frac{\rho_p}{18}\frac{d_p^2}{\mu}\frac{g}{V}$) are <1, where f is the drag factor, ρ_p the particle density (kg m^{-3}), d_p the particle diameter (m), μ the dynamic viscosity (Pa s), V (m s^{-1}) and L (m) the characteristic velocity and length for the flow, and g the acceleration due to gravity (m s^{-2}).

Gravitational instabilities have often been observed in many volcanic plumes and clouds, such as those associated with the eruption of Mount St. Helens 1980 (USA), Montserrat 1997 (West Indies), Eyafjallajökull 2010 (Iceland), Ruapehu 1996 (New Zealand) and Etna 2013 (Italy) (Bonadonna et al., 2002; Bonadonna et al., 2005a; Bonadonna et al. 2005b; Bonadonna et al., 2011; Durant et al., 2009; Manzella et al., 2015; Schultz et al., 2006) (e.g. Figure 1). In recent decades, several authors have used laboratory experiments to study the effects of gravitational instabilities on tephra sedimentation. For example, Carey (1997) examined the settling behaviour of volcanic ash (20-180 μm diameter) onto a water surface based on an experimental apparatus. The experimental set-up consisted of a 1.5-m-high settling column positioned over a 30 cm x 30 cm x 70 cm glass tank filled with water. Particles fell at a constant rate at the top of the column, accumulated on the water surface and then descended into the tank where they were photographed. Carey (1997) observed that the formation of fingers is directly linked to the reduction of particle settling velocity at the air-

water interface, which increases the concentration at the boundary layer. He also proved that the particle settling in the water column was accelerated by the formation of diffuse vertical gravity currents driven by gravitational instabilities that reduced the residence time of fine ash. Carazzo and Jellinek (2012) studied gravitational instabilities in volcanic plumes through both laboratory experiments and theoretical considerations. They found that finger formation reduced the residence time of fine ash into the gravitationally unstable particle boundary layer of volcanic clouds. Gravitational instabilities could therefore explain the unusual patterns of some tephra deposits (e.g. Bonadonna et al., 2002; Bonadonna et al., 2005) and/or the premature sedimentation of fine ash that are often explained by particle aggregation (e.g. Carey and Sigurdsson, 1982).

Models of sedimentation associated with gravitation instabilities were developed by Hoyal et al. (1999), recently modified by Manzella et al. (2015). Their formulation builds on the mass balance equation between the incoming and outcoming flux at the density interface for two different conditions: an upper quiescent layer (i.e. no external forcing of the fluid motion) and an upper turbulent layer (i.e. external forcing of the fluid motion). Furthermore, Cardoso and Zarrebini (2001) analysed buoyant particle-laden flows both experimentally and theoretically. They found that the development of particle-rich fingers was related to unstable particle stratification and that both the concentration of particles at the source of the plume, as well as the size of the particles, had notable influence on the sedimentation pattern in the environment below the surface current. Recently, Manzella et al. (2015) analysed gravitational instabilities during the 2010 eruption of Eyjafjallajökull volcano (Iceland) that transported fine ash to the ground at a speed of ~1 m/s, various orders of magnitude faster than the predicted terminal fall velocities of the smallest observed particles. These results were confirmed by specific laboratory experiments using glass beads in a density-stratified aqueous solution. They also showed how particle aggregation was strongly linked with sedimentation driven by fingers. The relationship between particle aggregation and gravitational instabilities was also suggested by Carazzo and Jellinek (2012).

Particle Imaging Velocimetry (PIV) is a widely used technique in fluid dynamics. It enables measuring the velocity of a fluid through the tracking of several particles able to reflect the light of a laser sheet (e.g. Adrian, 1991; Adrian, 1995; Adrian, 2005; Grant, 1997; Raffel et al., 2007). In volcanology, the PIV technique has already been applied to characterize plume dynamics, to measure the flow velocity for various ranges of particle size, overpressure ratios and densities and to analyse the effect of collision kinetic energy and atmospheric water vapour in subsaturated condition on ash aggregation (e.g. Saffaraval et al., 2012, Telling and Dufek, 2012, Chojnicki et al., 2014, Chojnicki et al., 2015a, Chojnicki et al., 2015b).

In our experiments, particles generating fingers are embedded in the fluid and, thanks to their potential for reflecting laser light, are used as PIV trackers. Experiments are carried out and analysed by the PIV technique (Section 2) in order to investigate the influence of particle size, composition and concentration on the formation and dynamics of the fingers (Section 3). Experimental results are then discussed and compared with observations of fingers occurring during explosive volcanic eruptions (Section 4).

2. METHODS

2.1 Experimental setup

Our experimental set-up is described in details by Manzella et al. (2015). The set-up comprises a Plexiglas tank of 30.3 cm x 50 cm x 7.5 cm (with *x* corresponding to the length (L), *y* to the height (H) and *z* to the width (W)) equipped with a removable sheet for the partition of two separate layers (Figure 2). The upper partition (H1 = 13.5 cm), which is filled with water and particles, is characterized by an initial lower density than the lower partition (H2 = 25.1 cm) that consists of a solution of water and sugar. The lower layer density was fixed with a value of 1008.4 kg/m^3, while variations in the density in the upper layer depend on the concentration and on the different densities of particles and, in our experiments, range between 999.8 and 1001.5 kg/m^3 (see Manzella et al. (2015) as GSA data repository for the formulation). The experiments are carried out under

136 isothermal conditions and the configuration is suitable to represent the state in which the plume and
137 fingers are advected at wind speed and the dynamic conditions are similar to those in volcanic
138 clouds (Manzella et al., 2015). The experiments entail removing the horizontal barrier that separates
139 the two fluids, and then observing the instabilities formed at the boundary of the two layers
140 propagating downward (Manzella et al., 2015). Similarly, we consider two different set-ups defined
141 as unmixed and mixed conditions. During unmixed experiments, particles are fully suspended
142 before the beginning of the experiment but they do not undergo additional external stirring once the
143 experiment starts, while, during mixed experiments, particles are continuously mixed with a rotary
144 stirrer that is stopped 1-2 seconds before the removal of the separation between the two layers (see
145 also Figure DR4 of the repository material of Manzella et al. (2015)). The stirrer is set at a speed of
146 30 rpm with a paddle of 6.9 cm (length) by 3.4 cm (diameter).

147 Experiments were carried out to examine the fluid dynamics associated with finger formation
148 using a PIV measuring system and image analysis. To this end, we recorded the experiments with a
149 high speed/high definition camera while a 2 Watt Neodymium-doped YAG (Yttrium Aluminium
150 Garnet) laser (RayPower 2000 by Dantec Dynamics), located at about 1 m from the frontal tank
151 wall, generates a green light to illuminate the particles used as tracer for the PIV analysis (Figure 2).
152 We were then able to measure the number and speed of fingers by image analysis and, therefore, to
153 assess the effect of concentration, size and particle composition on their generation and dynamics.

154 *2.2 Experimental conditions*

155 Particles used in our experiments include 4 grain-size classes of Glass Beads (GB), i.e. with
156 diameter < 32 μm, between 32-45 μm, between 45-63 μm, and between 63-90 μm as well as 6
157 grain-size classes of Andesitic, Rhyolitic, and Basaltic Volcanic Ash (Andes-VA; Rhyol-VA;
158 Basalt-VA, respectively), i.e. with diameter < 32 μm, 32-45 μm, 45-63 μm, 63-90 μm, 90-125 μm,
159 and 125-180 μm (Table 1). An additional class was also considered, where we mixed all the
160 particles with diameter <125 μm (called <125 μm in Table 1) to study the effect of using a widely
161 polydisperse mixture. Populations of different particle size were obtained through mechanical

sieving at the University of Geneva and the above-mentioned grain-size classes have been named after the sieves used which follow the international standard classification ISO3310. Laser diffraction analyses carried out with the CILAS 1180 instrument on selected samples indicate a good sorting inside the considered ranges (Folk and Ward, 1957).

For the andesitic composition, we used samples of volcanic ash erupted during the 2010 eruption of Eyjafjallajökull volcano (Iceland). This eruption produced a continuous volcanic plume up to 10 km above sea level between 14 April and 21 May 2010 (Gudmundsson et al., 2012). Glass composition ranges from benmoreite to trachyte with a silica content between 56 and 68 wt% and a total alkali from 7.3 and 9.1wt% (Cioni et al., 2014). The ash considered in our experiments was sampled between 4 and 8 May 2010 (Bonadonna et al., 2011). For the rhyolitic composition, we used samples of volcanic ash erupted during the May 2008 eruption of Chaitén volcano (Chile) (Alfano et al., 2011; Alfano et al., 2012; Alfano et al., 2016). The bulk magma composition of the main phase of this eruption varies between 73.0 and 75.5 wt% of SiO_2 (Alfano et al., 2011). Finally, for the basaltic composition, we used samples of volcanic ash from the 1992 eruption of Cerro Negro (Nicaragua) that lasted for about 21 days and was associated with a volcanic plume up to about 7 km a.s.l. (e.g. Connor and Connor, 2006; Connor et al, 1993). The silica content varies between 48.64 and 52.15 wt% (Roggensack et al., 1997). The density of individual size classes is complex to determine; however, based on the detailed analysis of Eychenne and Le Pennec (2012), we can assume that the density of fine ash is close to their Dense Rock Equivalent (DRE) value. The mean DRE value (measured with a helium pycnometer) of Eyjafjallajökull, Chaitén and Cerro Negro ash is 2738 kg m^{-3} (Bonadonna et al. 2011), 2240 kg m^{-3} (Alfano et al. 2012) and 2988 kg m^{-3} (measured for this work), respectively.

Three concentrations were considered to generate fingers: *C1* = 3 g/l, *C2* = 4 g/l, *C3* = 5 g/l. The concentrations were chosen based on experimental constraints as reported in Manzella et al. (2015). In fact, both lower and higher concentrations are not detectable experimentally based on the grey scale measuring strategy. The particle volumetric concentration in the experiments is then in the

188 order of 10^{-9}, which, together with their capacity to reflect the laser light, confirms that the particles
189 used can be exploited as tracers in PIV analysis. This is also supported by the fact that they are
190 coupled with the fluid since both their Stokes and Sedimentation numbers are < 1 (i.e. they are in
191 the range of 10^{-4}-10^{-1} and 0.5-1, respectively) for the grain-size and particle composition analysed in
192 our experiments (Carazzo and Jellinek, 2012). A detailed list of experiments is reported in Table 1.
193 In unmixed conditions, different tests were carried using GB with different concentrations
194 (experiment 1-10), GB with different sizes (experiments 11-17), Andes-VA with different sizes
195 (experiments 18-24) and Andes-VA with different concentrations (experiments 25-26). Experiments
196 with mixed conditions were carried out only for GB and Andes-VA in the range between 45 and 63
197 μm (experiments 28-29) and for Andes-VA with diameter < 125 μm (experiments 27 and 30).
198 However, the experiment 27 did not provide a good PIV analysis and was not considered for further
199 analysis. Experiments were finally carried out for Rhyol-VA and Basalt-VA with all the grain size
200 classes considered (experiments 31-34) in unmixed conditions. Experiments with GB were repeated
201 up to three times to verify the repeatability of the measurements (e.g. experiments 12-13, 14-15 and
202 16-17), while experiments with volcanic ash were carried out only once because of the limited
203 amount of material available. It is worth mentioning that GB particles are more visible than
204 volcanic ash particles, reflecting the laser light more efficiently. Among volcanic particles, the
205 Andes-VA ones reflect the laser light best and therefore, once the effect of the composition has
206 been studied, these were preferred for tests with volcanic ash.

207 *2.3 Data analysis*

208 Images of 1624 x 1600 pixel sizes were taken at of 0.03 s time steps and each particle captured by
209 the camera that scattered the laser light was used for the PIV analysis with the Dynamic Studio
210 Software (DANTEC, http://www.cefd-imech.ac.vn/lab/3D_PIV/DynamicStudio%20Manual.pdf).
211 PIV technique is based on the fact that the image intensity field at each instant corresponds to the
212 position of the particles reflecting the laser light and it assumes that between two instants t and t +
213 Δt, i.e. two consecutive exposures to the laser light, all particles inside a previously defined

interrogation window have moved together with the fluid with the same displacement vector, ΔX. This interrogation area (IA) should be small enough to respect this assumption but large enough to contain at least 10 particles reflecting the laser light to evaluate the intensity field. On the other hand, the particle volume fraction should be smaller than 10^{-4}, so that they are easily visible and do not influence the fluid flow. For this reason, in order to find the most suitable interrogation window and thus increase the accuracy of the analysis, the Dynamic Studio Software uses an iterative process that reduces the size of the interrogation area progressively from 128x128 to 16x16 pixels. In this framework, using a spatially statistical cross-correlation function which relates the difference in image intensity between two instants, we are able to evaluate the displacement of the fluid and the velocity vector for each interrogation area (Raffel et al., 2007). In addition, the DANTEC software is also used to evaluate the finger speed (m/s) measuring the position of the finger front at different times, the divergence (s^{-1}) and the vorticity (s^{-1}) fields.

As also described in the Dynamic Studio software manual, the divergence of a 3D vector velocity field $\overline{U}$ is defined as:

$$div(\overline{U}) = \frac{\partial U}{\partial x} + \frac{\partial V}{\partial y} + \frac{\partial W}{\partial z}. \quad (1)$$

For planar data gradients, as the one analysed with PIV, it reduces to:

$$div(\overline{UV}) = \frac{\partial U}{\partial x} + \frac{\partial V}{\partial y} \quad (2)$$

with *x*, *y* and *z* indicating the axis associated with the length, height, and width in Figure 2. Non-zero divergence values could indicate local changes in density and, therefore, local changes of particles concentration or, when the fluid is incompressible, a non-negligible variation of the velocity in the z direction.

Vorticity is a vector quantity, which corresponds to the rotation of the fluids. For planar data gradient only the z-component of vorticity, ω_z, can be calculated:

$$\omega_z = \frac{\partial V}{\partial x} - \frac{\partial U}{\partial y}. \quad (3)$$

According to Tritton (1988), turbulent flows are characterised by non-zero, fluctuating vorticity. Even if the studied gravitational instabilities cannot be considered two-dimensional because they have a component in the out of plane direction (z = W in Figure 2), this component is significantly smaller than the longitudinal (x = L in Figure 2) and vertical (y = H in Figure 2) dimensions of the tank, i.e. a few millimetres versus tens of centimetres. In addition, a single finger is mostly axi-symmetrical with respect to the flow direction, so we can assume that what we observe in a single finger in the x-y plane would be similar to what we could observe in the y-z plane. As a result, we consider that the PIV two-dimensional analysis can globally capture the main flow dynamics involved in the gravitational instabilities.

3. RESULTS

Figure 3 shows selected images of the experiments using GB and Andes-VA particles between 32 and 45 μm and between 63 and 90 μm with C1 as concentration and in unmixed condition (experiments 11, 15, 20 and 22 in Table 1). Fingers are clearly visible a few seconds (> 3s) after the sheet is removed and are of approximately the same size in each experiment.

Our analysis shows that the descending fingers have an irregular shape during the formation stage, and descend with large caps at their tips (e.g. Figure 3). The number of fingers increases with particle concentration (Figure 4a), but does not depend on the particle size and composition (Figure 4b). The mean wavelength, given by L/n where L is the length of the box (30.3 cm) and n is the number of fingers, ranges between 2.2 and 2.9 cm. Finger speed has a poor dependence on the particle concentration in the range of concentration investigated here (Figure 4c) and increases with particle size (Figure 4d). The experimental error bars in Figures 4a and 4b was evaluated by the standard deviation obtained from the mean value of finger number in ten images taken 3 s after removing the sheet. The mean and standard deviation in Figures 4c and 4d are instead evaluated by the analysis of five fingers over the course of one whole experiment.

It is worth mentioning that particles greater than 125 μm did not generate fingers (experiment 18 in Table 1). The number of fingers also depends on the experimental conditions of the upper layer. Figures 5a and 5b illustrate experiments with a "mixed" upper layer using GB and Andes-VA between 45 and 63 μm (experiments 28 and 29 in Table 1) showing a higher number of fingers (2-3 fingers more for both cases) with respect to "unmixed" experiments. Finger speed, instead, is independent of initial mixing.

We also analysed the evolution of finger dynamics with time. In general, the downward movement of fingers was not steady and we observed similar oscillations to those reported in Carazzo and Jellinek (2012). For the same class size, we found a general decrease of finger number with time mainly at the interface due to the decrease of the particle concentration in the upper layer. As an example, the experiment 11 in Table 1 (i.e. GB with size between 32-45 μm) shows 11 and 8 fingers, respectively, 5 and 30 s after the sheet was removed (Figures 6a and b). The speed of fingers is about 4.5 ±1.1 mm/s and 2.4 ± 0.2 mm/s after about 7 and 20 s, respectively. This behaviour was similar for different class sizes (e.g. Figures 6c and 6d). Figure 7 shows the variation of the finger number with respect to time for GB between 45 and 63 μm (experiment 3). At the beginning of the experiment, the number of fingers is 11±1 and after about 30 s the number of fingers remains almost constant (between 7±1 and 6±1). A power law fits the evolution with time well (R^2=0.88; Figure 7). We found that the finger speed was 4.6 ± 1.1, 3.0 ± 1.0 and 2.4 ± 1.3 mm/s at 10 s, at 20 s and 30 s, respectively. The study of finger evolution with time was also carried out for Andes-VA particles (experiments 19, 29, and 30) and for volcanic ash with a wide range of size (< 125 μm) showing similar trends. As an example, Figure 8 shows the experiment 24 in Table 1 carried out with Andes-VA. At the beginning of the experiment (< 10 s), fingers contain particles with the widest size range. In fact, even though particle size cannot be quantitatively assessed with PIV, a qualitative assessment can be made based on backscattering because larger particles show a smaller backscattering of the laser light and are less visible in the images retrieved by the camera

than smaller particles. In agreement with our previous observations, this experiment also shows how both the number and speed of fingers decrease with time. In particular, we observe 12 and 11 fingers after 5 and 10 s and 9 and 8 fingers after 15 sec and 20 s, respectively. The associated speed is 7.9 ± 1.2, 6.1 ± 1.0, 4.6 ± 1.7 and 4.3 ± 0.8 mm/s after 5, 10, 15 and 20 s, respectively.

Finally, we investigated the divergence and vorticity fields for GB and Andes-VA with different particle size and, in general, we found that divergence was zero everywhere except at the interface and inside the fingers. Figure 9 shows how the highest variation of the relative values of divergence and vorticity are concentrated in the fingers, where we also notice an increase of the brightness coming from the laser reflection of the particles (Figure 9a). An increase in brightness is hence associated with an increasing number of reflecting particles. As aforementioned, a non-zero divergence for PIV planar data could be associated with a significant velocity component along the out of plane direction (width in Figure 2), which cannot be excluded considering the 3D nature of fingers. However, the occurrence of the highest variations in divergence, even if small, combined with an increase of brightness within the fingers (Figures 9a and 9b), could suggest a temporary and localized variation in particle concentration. By contrast, a fluctuation of vorticity values in the *x-y* plane can be associated with a turbulence motion regardless of the 3D nature of the fingers. We can then infer that gravitational instabilities could be likely associated with an increase of concentration and turbulence with respect to initial conditions.

4. DISCUSSION

Our experiments confirm previous findings that gravitational instabilities have a marked effect on the sedimentation of volcanic ash (e.g. Carazzo and Jellinek, 2012; Manzella et al., 2015) and the analysis of these instabilities provide new insights into the effect of particle concentration, size and composition and into the evolution of fingers with time. Based on the analysis of divergence and vorticity, the formation of gravitational instabilities also has implications on particle aggregation.

313 Results show how the number of fingers depends largely on particle concentration in the upper
314 layer, as already concluded by Hoyal et al. (1999), while finger speed mostly depends on particle
315 size. Even though basaltic particles were more difficult to analyze than silicic particles due to their
316 dark colour that does not reflect the laser light well, particle composition seems to play a negligible
317 role on finger dynamics (e.g. Figure 4).

318 We have also shown how the number of fingers decreases with a drop in particle concentration
319 in the upper layer of the tank. Hence, there must be a critical value of particle concentration below
320 which fingers cannot form. In this sense, our experimental observations suggest that only volcanic
321 clouds characterized by a relatively high mass load of particles, and, therefore, volcanic eruptions
322 associated with a large Mass Eruption Rate (MER), are likely to form gravitational instabilities. As
323 an example, gravitational instabilities were clearly observed during the 23rd November 2013
324 explosive event of Etna volcano (Italy) that was characterized by a MER of about 10^5 kg/s
325 (Andronico et al., 2015) (see Figure 1a). The eruptive plume of the 4th May 2010 Eyjafjallajökull
326 eruption (Iceland) (Manzella et al., 2015) and of the 17th June 1996 eruption of Ruapehu volcano
327 (New Zealand) (Bonadonna et al., 2005), which generated well-developed gravitational instabilities,
328 were also characterized by a MER of about 10^5 kg/s (e.g. Degruyter and Bonadonna, 2013; Ripepe
329 et al., 2011; Bonadonna et al., 2005) (see Figures 1b and 1c). Gravitational instabilities were also
330 observed at the bottom of volcanic clouds associated with the thermal plumes of the August-
331 October 1997 Vulcanian explosions of Montserrat volcano, which injected an average of about 10^8-
332 10^9 kg of tephra into the atmosphere in just a few seconds (Bonadonna et al., 2002) (Figure 1d). By
333 contrast, gravitational instabilities were not observed during the 2011 and 2012 explosive events of
334 Etna volcano that were characterized by a lower MER (~10^4 kg/s) (Andronico et al., 2014).

335 Another fundamental condition for the formation of gravitational instabilities in volcanic clouds
336 is the presence of fine ash. Indeed, gravitational instabilities only formed in our experiments in
337 association with the sedimentation of particles <125 μm. Our results match those reported by Carey
338 (2007), although he used a different set-up and different concentration, but similar particle

composition (i.e. 1991 Pinatubo dacitic tephra) and fluid (i.e. water). In addition, both sets of experiments were performed in water, and, therefore, the critical cut-off size of 125 μm could be even smaller in air (Carazzo and Jellinek, 2012). All previously mentioned eruptions (i.e. Etna 23 November 2013, Eyjafjallajökull 2010, Montserrat 1997 and Ruapehu 1996) were characterized by the presence of particles < 125 μm, i.e. ~6wt% for Ruapehu 1996, ~40wt% for Eyjafjallajökull 2010 and ~50-80wt% for the August-October 1997 Vulcanian explosions of Montserrat (Bonadonna et al., 2002; Bonadonna and Houghton 2005; Bonadonna et al., 2011). In addition, volcanic lightning that is typically associated with particle-laden jet and abundance of fine particles (Cimarelli et al., 2013), was observed during the 23 November 2013 Etna eruption.

Theory reported in Manzella et al. (2015) shows how an increase in particle concentration in the upper layer would increase g', and, therefore, the finger speed. In fact, finger velocity is equal to: $v_f = g'^{\frac{2}{5}}(v_p \frac{1}{4}\pi\delta^2)^{1/5}$, where v_p is the particle settling velocity, δ is the Particle Boundary Layer (PBL) thickness, g' is the reduced gravity of the PBL given by $g' = g\frac{\rho_{PBL}-\rho_a}{\rho_a}$, where g is the gravity and ρ_{PBL} and ρ_a are the density of PBL and of the atmosphere, respectively. As a result, the higher the particle concentration in volcanic plumes, the higher the finger speed. Although we investigated a small range, a slight increase of the finger speed with concentration is also confirmed by our experiments and by theory (e.g. Hoyal et al., 1999). This aspect should however be explored further by enlarging the concentration range. Moreover, the theory of Hoyal et al. (1999) can explain the observed increase of particle speed with particle size and the negligible effect of particle composition on finger dynamics. First, the larger the particle size, the larger the particle velocity v_p, and, therefore, the finger velocity v_f. Second, the main difference among the particle composition is the variation in density that, however, is negligible for particles < 125 μm (e.g. Bonadonna and Phillips, 2003; Eychenne and Le Pennec, 2012). In fact, the difference in DRE values is only between 2240 kg/m^3 for Chaitén rhyolitic ash and 2988 kg/m^3 for Cerro Negro basaltic ash. Furthermore, volcanic clouds represent a polydisperse mixture containing a wide range of particle

sizes even at medial-distal locations. Based on our results and theory, we expect that i) the number of fingers decreases with the distance from the vent and ii) the finger speed decreases with the distance from the vent for a combined effect of the reduction of both volcanic ash concentration and particle size in the upper layer.

Aggregation of ash particles into clusters with a higher terminal fall velocity leads to a reduction of the atmospheric lifetime (e.g. Brown et al., 2012; Costa et al., 2006; Durant, 2015). It has already been suggested that aggregation could be enhanced inside the fingers due to the high particle concentration (e.g. Carazzo and Jellinek, 2012). Our analysis of divergence and vorticity provides additional evidence that indicates the potential role of gravitational instabilities in forming particle aggregates. Fluctuations of divergence and vorticity inside the fingers could represent an increase of particle concentration and turbulence with respect to the surrounding regions, which increases the probability of collisions, and, therefore, promotes aggregation. Nonetheless, the formation of ash clusters within volcanic plumes and clouds and the sedimentation of single ash clusters independently of gravitational instabilities cannot be excluded, in particular when the cluster settling velocity is higher than the finger settling velocity (e.g. Manzella et al., 2015).

Finally, our results clearly show that the highest values of finger number and finger speed are associated with their initial formation and both decrease with time. This could be related to the decrease of particle concentration in the upper layer, which in our experiment progressively decreases with time. However, during an eruption, volcanic plumes are continuously fed at the eruptive vent and the decrease in finger number and speed could only occur at the end of the explosive activity. This also supports the idea that particle aggregation may be more efficient at the beginning of finger formation when the concentration is the highest.

5. CONCLUSIONS

A comprehensive physical characterization of the sedimentation processes occurring in volcanic plumes and clouds relies on a better understanding of the gravitational instabilities. We carried out

experiments using a Plexiglas tank of 50 cm x 30.3 cm x 7.5 cm equipped with a horizontal removable plastic pet sheet to separate the two layers. The upper layer was made up of water and particles, while the lower layer was a solution of water and sugar that was initially denser than the upper layer. After removing the horizontal plastic pet sheet, particles were illuminated with a laser and filmed with a HD camera and analysed by PIV. Our experimental investigations provide new insights into the mechanisms characterizing finger formation and finger dynamics. In particular:

1) Number of fingers and finger speed increase with particle concentration in the upper layer; this is in agreement with previous experimental observations (e.g., Carazzo and Jellinek, 2012; Manzella et al., 2015) and supports field observations, where fingers have been observed only in volcanic plumes with relatively high MER (i.e. MER$\geq 10^5$ kg/s);
2) Gravitational instabilities were observed only with particles <125 μm; this also concurs with previous experimental observations (i.e. Carey 2007; Carazzo and Jellinek, 2012) and confirms the idea that a relative abundance of fine ash is necessary to generate fingers. However, the size cut-off in air could be smaller due to different buoyancy;
3) Number of fingers and finger speed are independent of particle composition, suggesting that finger formation can occur independently of magma composition;
4) The relation between gravitational instabilities and particle aggregation was explored based on the analysis of divergence and vorticity inside the fingers. These values suggest heterogeneity in particle concentration and an increase in turbulent motion that need further exploration with experiments including the analysis of the 3D component. Given that a high concentration of particles <125 μm and turbulence are both factors promoting aggregation, we can conclude that particle aggregation could easily occur both at the base of the cloud where fingers form and inside fingers.

Acknowledgments

The authors are grateful to M. Prestifilippo and E. Rossi for the useful discussions, to L. Pioli, and J. Ruch for their help during the experiments at the Geneva laboratory and to F. Arlaud for technical support. The work was funded by the ESF Research Networking Programmes, Reference N°4257 MeMoVolc, by the project 'From observations to experiments: Describing and characterizing gravitational instabilities of volcanic plumes'. The contribution of C. Bonadonna was supported by the Swiss National Science Foundation project No 200021_156255. We thank James White (Executive Editor), Joe Dufek (associate Editor), David Jessop and one anonymous reviewer for their constructive comments that greatly improved the manuscript.

Figures and Table Captions

Figure 1. Gravitational instabilities associated with:

a) 23 November 2013 lava fountain of Etna volcano, Italy (photo by http://www.tboeckel.de/EFSF/efsf_etna/Etna2013/Etna_11_13/volcano_etna_11_2013_e.htm); b) Eyjafjallajökull plume on 4 May 2010, Iceland (photo by C. Bonadonna); c) 17 June 1996 eruption of Ruapehu volcano, New Zealand (photo from http://www.natgeocreative.com/photography/1302290); d) Vulcanian explosion in September 1997, Montserrat (photo adjusted from Bonadonna et al. (2002)).

Figure 2. Experimental set-up comprising a Plexiglas tank of 30.3 cm x 50 cm x 7.5 cm (*x* corresponding to the length (L) direction, *y* to the height (H), *z* to the width (W)), a removable pet sheet, a laser and a HD camera. Particles, HD Camera, and laser instrument are not to scale. The stirrer used in our mixed experiments is shown in Figure DR4 of the repository material of Manzella et al. (2015).

Figure 3. Images of experiments with: a) GB with diameter between 32-45 μm (experiment 11 in Table 1); b) GB with diameter between 63-90 μm (experiment 15 in Table 1); c) Andes-VA with diameter between 32-45 μm (experiment 22 in Table 1); and d) Andes-VA with diameter between 63-90 μm (experiment 20 in Table 1). Images (26 cm x 16.5 cm) are taken about 10 seconds after removing the horizontal pet sheet separating the two fluids in unmixed conditions.

Figure 4. Plots showing the number of fingers with respect to: a) particle concentration in the upper layer (g/l) for GB and Andes-VA and b) particle size (μm) for GB, Andes-VA, Rhyol-VA and Basalt-VA; and the speed of fingers with respect to: c) particle concentration in the upper layer (g/l) for GB, Andes-VA, and Theory (Hoyal et al., 1999) and d) particle size for GB and Andes-VA (μm) (experiments 19 to 26 and 31 to 43 in Table 1).

Figure 5. Images (26 cm x 16.5 cm) showing the number of fingers for the experiments with a mixed upper layer using a) GB between 45 and 63 μm (experiment 28 in Table 1) and b) Andes-VA between 45 and 63 μm (experiment 29 in Table 1).

Figure 6. Images (26 cm x 16.5 cm) of experiments with GB of diameter between 32-45 μm (experiment 11 in Table 1) taken a) 5 s and b) 30 s and of diameter between 45-63 μm (experiment 3 in Table 1) taken c) 5 s and d) 30 s after removing the horizontal pet sheet. Arrows indicate observed fingers.

Figure 7. Plot showing the evolution of the finger number with time for GB between 45-63 μm (experiment 3 in Table 1).

Figure 8. Images (26 cm x 16.5 cm) of experiment 24 in Table 1 that includes Andes-VA with a wide range of particle sizes (< 125 μm) imaged about a) 5 s, b) 10 s, c) 15 s, and d) 20 s after removing the horizontal pet sheet.

Figure 9. Image of the experiment 7 (Table 1) for GB between 45-63 μm a) after 15 s the finger formation; b) divergence (s^{-1}) and c) vorticity (s^{-1}) fields and d) divergence and vorticity values measured along the orange line across the finger in c).

Table 1. Summary of experiments: experiment number; particle composition including glass beads (GB), andesitic volcanic ash (Andes-VA), rhyolitic volcanic ash (Rhyol-VA), and basaltic volcanic ash (Basalt-VA); particle size (S) in μm; Concentration in g/l; the upper layer was both quiescent (i.e. unmixed experiments, or continually mixed using a rotary stirrer (i.e. mixed experiments) described in Manzella et al. (2015).

References

Adrian RJ (1991) Particle-imaging techniques for experimental fluid mechanics. Annu. Rev. Fluid Mech. 23:261–304

Adrian RJ (1995) Limiting resolution of particle image velocimetry for turbulent flow. Advances in Turbulence Research Pohang Korea 1-19 Postech

Adrian RJ (2005) 20 years of particle image velocimetry. Exp Fluids 39:159–69

475 Alexander D (2013) Volcanic ash in the atmosphere and risks for civil aviation: a study in European
476 crisis management. Int. J. Disaster Risk Sci. 4: 9–19
477 Alfano F, Bonadonna C, Volentik ACM, Connor CB, Watt SFL, Pyle DM, Connor LJ (2011)
478 Tephra stratigraphy and eruptive volume of the May, 2008, Chaiten eruption, Chile. Bull
479 Volcanol 73 (5): 613–630
480 Alfano F, Bonadonna C, Gurioli, L (2012) Insights into eruption dynamics from textural analysis:
481 the case of the May, 2008, Chaitén eruption. Bull Volcanol doi:10.1007/s00445-012-0648-3
482 Alfano F, Bonadonna C, Watt S, Connor C, Volentik A, Pyle DM (2016) Reconstruction of total
483 grain size distribution of the climactic phase of a long-lasting eruption: the example of the 2008–
484 2013 Chaitén eruption, Bull Volcanol, 78:46, doi:10.1007/s00445-016-1040-5
485 Andronico D, Scollo S, Lo Castro MD, Cristaldi A (2014) Representivity of incompletely sampled
486 fall deposits in estimating eruption source parameters: a test using the 12–13 January 2011 lava
487 fountain deposit from Mt. Etna volcano, Italy. Bull Volcanol (2014) 76:861 doi:10.1007/s00445-
488 014-0861-3
489 Andronico D, Scollo S, Cristaldi A (2015) Unexpected hazards from tephra fallouts at Mt Etna: The
490 23 November 2013 lava fountain. Journal Volcanololgy Geothermal Research 204: 118-125
491 Blong, R., 2000, Assessment of volcanic risk, in Sigur, H., et al., eds., Encyclopedia of Volcanoes:
492 San Diego, Academic Press, p. 1215–1225. Bonadonna C, Macedonio G, Sparks RSJ (2002)
493 Numerical modelling of tephra fallout associated with dome collapses and Vulcanian explosions:
494 application to hazard assessment on Montserrat. Geological Society London Memoir 2002
495 Bonadonna C, Mayberry GC, Calder ES, Sparks RSJ, Choux C, Jackson P, Lejeune AM, Loughlin
496 SC, Norton GE, Rose WI, Ryan G, Young SR (2002) Tephra fallout in the eruption of Soufrière
497 Hills Volcano, Montserrat. In: Druitt TH Kokelaar BP (eds) The eruption of Soufrière Hills
498 Volcano, Montserrat, from 1995 to 1999. Geological Society, London, Memoir, v. 21, p. 483-
499 516, doi:10.1144/GSL.MEM.2002.021.01.22

500 Bonadonna C, Phillips JC (2003) Sedimentation from strong volcanic plumes. J Geophys Res,
501 108(B7): 2340 doi:10.1029/2002JB002034
502 Bonadonna C, Houghton BF (2005) Total grain-size distribution and volume of tephra-fall deposits.
503 Bull Volcanol 67:441-456
504 Bonadonna C, Phillips JC, Houghton BF (2005a) Modeling tephra fall from a Ruapehu weak plume
505 eruption. J Geophys Res 110(B08209) doi:10.1029/2004JB003515
506 Bonadonna C, Connor CB, Houghton B.F, Connor L, Byrne M, Laing A, Hincks TK (2005b)
507 Probabilistic modeling of tephra dispersion: Hazard assessment of a multi-phase rhyolitic
508 eruption at Tarawera, New Zealand. J Geophys Res 110:B03203 doi:10.1029/ 2003JB002896
509 Bonadonna C, Genco R, Gouhier M, Pistolesi M, Cioni R, Alfano F, Hoskuldsson A, Ripepe M
510 (2011) Tephra sedimentation during the 2010 Eyjafjallajökull eruption (Iceland) from deposit,
511 radar, and satellite observations. J Geophys Res, 116, B12202, doi:10.1029/2011JB008462
512 Bonadonna C, Folch A, Loughlin S, Puempel H (2012) Future developments in modelling and
513 monitoring of volcanic ash clouds: outcomes from the first IAVCEI-WMO workshop on Ash
514 Dispersal Forecast and Civil Aviation. Bull Volcanol 74: 1-10
515 Brown RJ, Bonadonna C, Durant AJ (2012) A review of volcanic ash aggregation. Phys Chem
516 Earth A/B/C 45-46: 65-78
517 Carazzo G, Jellinek AM (2012) A new view of the dynamics, stability and longevity of volcanic
518 clouds. Earth Planet Sci Lett 325-326: 39–51
519 Carazzo G, Jellinek AM (2013) Particle sedimentation and diffusive convection in volcanic ash-
520 clouds. Journal Geophysical Research 118:1420-1437
521 Cardoso SSS, Zarrebini M (2001) Convection driven by particle settling surrounding a turbulent
522 plume. Chemical Engineering Science 56:3365–3375
523 Carey SN (1997) Influence of convective sedimentation on the formation of widespread tephra fall
524 layers in the deep sea. Geology 25: 839-842

525 Carey SN, Sigursson H (1982) Influence of particle aggregation on deposition of distal tephra from
526 the May 18, 1980, eruption of Mount St. Helens volcano. Journ Geophys Res 87: 7061-7072
527 Chojnicki KN, Clarke AB, Adrian RJ, Phillips JC (2014) The flow structure of jets from transient
528 sources and implications for modeling short-duration explosive volcanic eruptions. Geochem
529 Geophys Geosyst 15, 4831–4845
530 Chojnicki KN, Clarke AB, Phillips JC, Adrian RJ (2015a) Rise dynamics of unsteady laboratory
531 jets with implications for volcanic plumes' Earth and Planetary Science Letters 412: 186-196
532 Chojnicki KN, Clarke AB, Phillips JC, Adrian RJ (2015b) The evolution of volcanic plume
533 morphology in short-lived eruptions Geology 43:707-710
534 Cioni R, Pistolesi M, Bertagnini A, Bonadonna C, Hoskuldsson A, Scateni B (2014) Insights into
535 the dynamics and evolution of the 2010 Eyjafjallajökull summit eruption (Iceland) provided by
536 volcanic ash textures. Earth and Planetary Science Letters 394: 111-123
537 Cimarelli C, Alatorre-Ibargüengoitia MA, Kuppers U, Scheu B, Dingwell DB (2013) Experimental
538 generation of volcanic lightning. Geology doi:10.1130/G34802.1
539 Connor LJ, Connor CB (2006) Inversion is the key to dispersion: understanding eruption dynamics
540 by inverting tephra fallout. In:Mader H, Coles SG, Connor CB, Connor LJ (eds) Statistics in
541 volcanology. Geological Society, London, pp 231–242
542 Connor CB, Powell L, Strauch W, Navarro M, Urbina O, Rose WI (1993) The 1992 eruption of
543 Cerro Negro, Nicaragua: An example of Plinian-style activity at a small basaltic cinder cone.
544 Eos, Transactions of the American Geophysical Union, 74: 640
545 Costa A, Macedonio G, Folch A (2006) A three dimensional Eulerian model for transport and
546 deposition of volcanic ashes. Earth Planet. Sci. Lett. 241: 634–647
547 Degruyter W, Bonadonna C (2013) Impact of wind on the condition for column collapse of volcanic
548 plumes. 377: 218-226

549 Durant AJ; Rose WI (2009) Hydrometeor-enhanced tephra sedimentation: Constraints from the 18
550 May 1980 eruption of Mount St. Helens. Journal Geophysical Research 114: doi:
551 10.1029/2008JB005756
552 Durant (2015) Toward a realistic formulation of fine-ash lifetime in volcanic clouds Geology. 43:
553 271-272
554 Eychenne J, Le Pennec JL (2012) Sigmoidal particle density distribution in a subplinian scoria fall
555 deposit. Bull Volc 74:2243-2249
556 Elissondo M, Baumann V, Bonadonna C, Pistolesi M, Cioni R, Bertagnini A, Biass S, Herrero JC,
557 and Gonzalez R (2016) Chronology and impact of the 2011 Cordón Caulle eruption, Chile. Nat.
558 Hazards Earth Syst. Sci., 16: 675–704
559 Folch (2012) A review of tephra transport and dispersal models: Evolution, current status, and
560 future perspectives. Journal of Volcanology and Geothermal Research 235-236: 96-115
561 Folk RL and Ward WC (1957) Brazos River bar: a study in the significance of grain size
562 parameters. Journal of Sedimentary Petrology, 27: 3–26.
563 Grant I (1997) Particle image velocimetry: A review. Proceeding of the Institution of mechanical
564 engineers part C- Journal of Mechanical Engineering Science, 211, 1: 55-76
565 Gudmundsson MT, Thordarson T, Hoskuldsson A, Larsen G, Bjornsson H, Prata FJ, Oddsson B,
566 Magnusson E, Hognadottir T, Petersen GN, Hayward CL, Stevenson JA, Jonsdottir I (2012) Ash
567 generation and distribution from the April-May 2010 eruption of Eyjafjallajokull, Iceland.
568 Scientific Reports, 2: doi: 10.1038/srep00572
569 Hoyal D, Bursik MI, Atkinson JF (1999) Settling-driven convection: A mechanism of
570 sedimentation from stratified fluids. J Geophys Res 104 (C4): 7953-7966
571 Manzella I, Bonadonna C, Phillips JC, Monnard H. (2015) The role of gravitational instabilities in
572 deposition of volcanic ash. Geology 43: 211-214
573 Miller TP, Casadevall TJ (2000) Volcanic Ash Hazards to Aviation. Encyclopedia of Volcanoes.
574 Sigurdsson, H., Academic Press, San Diego, CA

575 Oxford Economics (2010) The Economic Impacts of Air Travel Restrictions Due to Volcanic Ash
576 Report for Airbus, available at: http://controverses.mines-
577 paristech.fr/public/promo10/promo10_G11/data/documents/Volcanic-Update.pdf
578 Raffel M,Willert C,Wereley S, Kompenhans J. (2007) Particle Image Velocimetry: A Practical
579 Guide. New York: Springer
580 Ripepe M, Bonadonna C, Folch A, Delle Donne D, Lacanna G, Marchetti E, Hoskuldsson A,
581 Hoeskuldsson A (2011) Ash-plume dynamics and eruption source parameters by infrasound and
582 thermal imagery: The 2010 Eyjafjallajokull eruption, Earth and Planetary Science Letters 366:
583 112-121
584 Roggensack K, Hervig R L, McKnight SB, Williams SN (1997) Explosive Basaltic Volcanism from
585 Cerro Negro Volcano: Influence of Volatiles on Eruptive Style. Science 277: 1639-1641
586 Saffaraval F, Solovitz SA, Ogden DE, Mastin LG (2012) Impact of reduced near-field entrainment
587 of overpressured volcanic jets on plume development, Journal of Geophysical Research 117:
588 B05209, doi:10.1029/2011JB008862
589 Sammons P, McGuire B, Edwards S (2010) Volcanic hazard from Iceland – analysis and
590 implications of the Eyjafjallajokull eruption, UCL Institute for Risk and Disaster Reduction
591 report, London, available at: https://www.ucl.ac.uk/rdr/documents/docs-publications-
592 folder/icelandreport
593 Schultz DM, Kanak KM, Straka JM, Trapp RJ, Gordon BA, Zrnic DS, Bryan GH, Durant AJ,
594 Garrett TJ, Klein PM, Lilly DK (2006) The mysteries of mammatus clouds: Observations and
595 formation mechanisms. Journal of the Atmospheric Sciences 63: 2409–2435
596 Scollo S, Tarantola S, Bonadonna C, Coltelli M, Saltelli A (2008) Sensitivity analysis and
597 uncertainty estimation for tephra dispersal models. Journal of Geophysical Research-Solid Earth,
598 113:B06202, doi:10.1029/2006JB004864

599 Scollo S, Folch A, Coltelli M, Realmuto VJ (2010) Three-dimensional volcanic aerosol dispersal: a
600 comparison between MISR data and numerical simulations. Journal of Geophysical Research-
601 Atmospheres 115:doi: 10.1029/2009JD013162
602 Telling J, Dufek J (2012) An experimental evaluation of ash aggregation in explosive volcanic
603 eruptions. Journal of Volcanology and Geothermal Research 209: 1-8
604 Tritton D J (1988) Physical Fluid Dynamics, Oxford University Press, Oxford
605 Turner JS (1979) Buoyancy effects in fluids: Cambridge, Cambridge University Press
606 Wilson T, Stewart C, Bickerton H, Baxter P, Outes V, Villarosa G, Rovere E. (2013) Impacts of the
607 June 2011 Puyehue- Cordón Caulle volcanic complex eruption on urban infrastructure,
608 agriculture and public health. GNS Science, New Zealand, GNS Science Report 2012/20: 88

Settling-driven gravitational instabilities associated with volcanic clouds: new insights from experimental investigations

Simona Scollo[1], Costanza Bonadonna[2], Irene Manzella[2]

Istituto Nazionale di Geofisica e Vulcanologia, Osservatorio Etneo, Sezione di Catania, Italy

Département des sciences de la Terre, Université de Genève, Suisse

Abstract

Downward propagating instabilities are often observed at the bottom of volcanic plumes and clouds. These instabilities generate fingers that enhance the sedimentation of fine ash. Despite their potential influence on tephra dispersal and deposition, their dynamics is not entirely understood, undermining the accuracy of volcanic ash transport and dispersal models. Here, we present new laboratory experiments that investigate the effects of particle size, composition and concentration on finger generation and dynamics. The experimental set-up consists of a Plexiglas tank equipped with a removable plastic sheet that separates two different layers. The lower layer is a solution of water and sugar, initially denser than the upper layer, which consists of water and particles. Particles in the experiments include glass beads as well as andesitic, rhyolitic, and basaltic volcanic ash. During the experiments, we removed the horizontal plastic sheet separating the two fluids. Particles were illuminated with a laser and filmed with a HD camera; the Particle Image Velocimetry (PIV) is used to analyse finger dynamics. Results show that both the number and the downward advance speed of fingers increase with particle concentration in the upper layer, while finger speed increases with particle size but is independent of particle composition. An increase in particle concentration and turbulence is estimated to take place inside the fingers, which could promote aggregation in subaerial fallout events. Finally, finger number, finger speed and particle concentration were observed to decrease with time after the formation of fingers. A similar pattern

could occur in volcanic clouds when the mass supply from the eruptive vent is reduced. Observed evolution of the experiments through time also indicates that there must be a threshold of fine ash concentration and mass eruption rate below which fingers do not form; this is also confirmed by field observations.

Key words: Tephra; Volcanic Plumes; Volcanic Ash; Laboratory Experiments; PIV Analysis; Particle Aggregation.

1. INTRODUCTION

During explosive volcanic eruptions, a large number of volcanic particles is injected into the atmosphere with the potential of generating significant hazards to nearby communities and various economic sectors. While fine ash in distal area may produce long-term health risks and is extremely dangerous for aircraft jet engines due to the accumulation of melted glass particles and erosion of turbine blades, proximal fallout can cause collapse of buildings and damage to agriculture, vegetation, lifelines, road networks and critical infrastructures (e.g. Blong, 2000; Miller and Casadevall, 2000). The volcanic crisis of Eyafjallajökull volcano (2010, Iceland) and Cordón Caulle volcano (2011, Chile), represent the most recent examples of widespread economic disruption caused by volcanic ash (e.g. Alexander, 2013; Oxford, 2010; Elissondo et al., 2016; Sammons et al., 2010; Wilson et al., 2013). Volcanic risk can be mitigated thanks to accurate forecasting of tephra dispersal that builds on a good understanding and description of volcanic plumes and cloud dynamics and sedimentation. There is a variety of volcanic ash dispersal models based on different assumptions and modelling strategies (see Folch et al. (2012) for a review). Sensitivity analyses have demonstrated that, when eruption source parameters are well constrained, eruptive phenomena such as particle dispersal and sedimentation can be reproduced with good accuracy (e.g. Costa et al., 2006; Scollo et al., 2010; Bonadonna et al., 2012). However, even after an accurate model calibration, differences between field data and model results can reach up to 150% (e.g. Scollo et al., 2008). Causes of these discrepancies include the fact that not all the physical processes of volcanic plumes and clouds are fully described. Among these processes, the generation and dynamics of fingers associated with settling-driven gravitational instabilities, also called convective instabilities, could play an important role (e.g. Carazzo and Jellinek, 2013; Durant, 2015; Manzella et al., 2015; Figure 1).

In the presence of particle-laden fluids, such as volcanic plumes and clouds, gravitational instabilities are induced by particle settling across the density interface (Hoyal et al., 1999). Initially the configuration is gravitationally stable: the lighter particle laden fluid (e.g. volcanic

current) is emplaced above the denser one (e.g. atmospheric layer). Small variations in density at different points of the interface occur due to particle settling, generating instabilities. As a consequence, vertical gravity currents, called fingers, start to develop in the lower layer and lead to convective motion (Turner, 1979), which drives the vertical transport of particles in the lower layer (e.g. Carazzo and Jellinek, 2012; Hoyal et al., 1999; Manzella et al., 2015). The main condition for the formation of settling-driven gravitational instabilities is that the particle suspension behaves as a continuum and this happens if the finger downward velocity has to be greater than particle settling velocity (Hoyal et al., 1999). This condition (e.g. the particles to be coupled with the fluid and efficiently mixed) is satisfied, according to Carazzo and Jellinek (2012), when both the Stokes number ($St = \frac{1}{f}\frac{\rho_p}{18}\frac{d_p^2}{\mu}\frac{V}{L}$) and the Sedimentation number ($\sum = \frac{1}{f}\frac{\rho_p}{18}\frac{d_p^2}{\mu}\frac{g}{V}$) are <1, where f is the drag factor, ρ_p the particle density (kg m^{-3}), d_p the particle diameter (m), μ the dynamic viscosity (Pa s), V (m s^{-1}) and L (m) the characteristic velocity and length for the flow, and g the acceleration due to gravity (m s^{-2}).

Gravitational instabilities have often been observed in many volcanic plumes and clouds, such as those associated with the eruption of Mount St. Helens 1980 (USA), Montserrat 1997 (West Indies), Eyafjallajökull 2010 (Iceland), Ruapehu 1996 (New Zealand) and Etna 2013 (Italy) (Bonadonna et al., 2002; Bonadonna et al., 2005a; Bonadonna et al. 2005b; Bonadonna et al., 2011; Durant et al., 2009; Manzella et al., 2015; Schultz et al., 2006) (e.g. Figure 1). In recent decades, several authors have used laboratory experiments to study the effects of gravitational instabilities on tephra sedimentation. For example, Carey (1997) examined the settling behaviour of volcanic ash (20-180 μm diameter) onto a water surface based on an experimental apparatus. The experimental set-up consisted of a 1.5-m-high settling column positioned over a 30 cm x 30 cm x 70 cm glass tank filled with water. Particles fell at a constant rate at the top of the column, accumulated on the water surface and then descended into the tank where they were photographed. Carey (1997) observed that the formation of fingers is directly linked to the reduction of particle settling velocity at the air-

water interface, which increases the concentration at the boundary layer. He also proved that the particle settling in the water column was accelerated by the formation of diffuse vertical gravity currents driven by gravitational instabilities that reduced the residence time of fine ash. Carazzo and Jellinek (2012) studied gravitational instabilities in volcanic plumes through both laboratory experiments and theoretical considerations. They found that finger formation reduced the residence time of fine ash into the gravitationally unstable particle boundary layer of volcanic clouds. Gravitational instabilities could therefore explain the unusual patterns of some tephra deposits (e.g. Bonadonna et al., 2002; Bonadonna et al., 2005) and/or the premature sedimentation of fine ash that are often explained by particle aggregation (e.g. Carey and Sigurdsson, 1982).

Models of sedimentation associated with gravitation instabilities were developed by Hoyal et al. (1999), recently modified by Manzella et al. (2015). Their formulation builds on the mass balance equation between the incoming and outcoming flux at the density interface for two different conditions: an upper quiescent layer (i.e. no external forcing of the fluid motion) and an upper turbulent layer (i.e. external forcing of the fluid motion). Furthermore, Cardoso and Zarrebini (2001) analysed buoyant particle-laden flows both experimentally and theoretically. They found that the development of particle-rich fingers was related to unstable particle stratification and that both the concentration of particles at the source of the plume, as well as the size of the particles, had notable influence on the sedimentation pattern in the environment below the surface current. Recently, Manzella et al. (2015) analysed gravitational instabilities during the 2010 eruption of Eyjafjallajökull volcano (Iceland) that transported fine ash to the ground at a speed of ~1 m/s, various orders of magnitude faster than the predicted terminal fall velocities of the smallest observed particles. These results were confirmed by specific laboratory experiments using glass beads in a density-stratified aqueous solution. They also showed how particle aggregation was strongly linked with sedimentation driven by fingers. The relationship between particle aggregation and gravitational instabilities was also suggested by Carazzo and Jellinek (2012).

Particle Imaging Velocimetry (PIV) is a widely used technique in fluid dynamics. It enables measuring the velocity of a fluid through the tracking of several particles able to reflect the light of a laser sheet (e.g. Adrian, 1991; Adrian, 1995; Adrian, 2005; Grant, 1997; Raffel et al., 2007). In volcanology, the PIV technique has already been applied to characterize plume dynamics, to measure the flow velocity for various ranges of particle size, overpressure ratios and densities and to analyse the effect of collision kinetic energy and atmospheric water vapour in subsaturated condition on ash aggregation (e.g. Saffaraval et al., 2012, Telling and Dufek, 2012, Chojnicki et al., 2014, Chojnicki et al., 2015a, Chojnicki et al., 2015b).

In our experiments, particles generating fingers are embedded in the fluid and, thanks to their potential for reflecting laser light, are used as PIV trackers. Experiments are carried out and analysed by the PIV technique (Section 2) in order to investigate the influence of particle size, composition and concentration on the formation and dynamics of the fingers (Section 3). Experimental results are then discussed and compared with observations of fingers occurring during explosive volcanic eruptions (Section 4).

2. METHODS

2.1 Experimental setup

Our experimental set-up is described in details by Manzella et al. (2015). The set-up comprises a Plexiglas tank of 30.3 cm x 50 cm x 7.5 cm (with *x* corresponding to the length (L), *y* to the height (H) and *z* to the width (W)) equipped with a removable sheet for the partition of two separate layers (Figure 2). The upper partition (H1 = 13.5 cm), which is filled with water and particles, is characterized by an initial lower density than the lower partition (H2 = 25.1 cm) that consists of a solution of water and sugar. The lower layer density was fixed with a value of 1008.4 kg/m^3, while variations in the density in the upper layer depend on the concentration and on the different densities of particles and, in our experiments, range between 999.8 and 1001.5 kg/m^3 (see Manzella et al. (2015) as GSA data repository for the formulation). The experiments are carried out under

136 isothermal conditions and the configuration is suitable to represent the state in which the plume and
137 fingers are advected at wind speed and the dynamic conditions are similar to those in volcanic
138 clouds (Manzella et al., 2015). The experiments entail removing the horizontal barrier that separates
139 the two fluids, and then observing the instabilities formed at the boundary of the two layers
140 propagating downward (Manzella et al., 2015). Similarly, we consider two different set-ups defined
141 as unmixed and mixed conditions. During unmixed experiments, particles are fully suspended
142 before the beginning of the experiment but they do not undergo additional external stirring once the
143 experiment starts, while, during mixed experiments, particles are continuously mixed with a rotary
144 stirrer that is stopped 1-2 seconds before the removal of the separation between the two layers (see
145 also Figure DR4 of the repository material of Manzella et al. (2015)). The stirrer is set at a speed of
146 30 rpm with a paddle of 6.9 cm (length) by 3.4 cm (diameter).

147 Experiments were carried out to examine the fluid dynamics associated with finger formation
148 using a PIV measuring system and image analysis. To this end, we recorded the experiments with a
149 high speed/high definition camera while a 2 Watt Neodymium-doped YAG (Yttrium Aluminium
150 Garnet) laser (RayPower 2000 by Dantec Dynamics), located at about 1 m from the frontal tank
151 wall, generates a green light to illuminate the particles used as tracer for the PIV analysis (Figure 2).
152 We were then able to measure the number and speed of fingers by image analysis and, therefore, to
153 assess the effect of concentration, size and particle composition on their generation and dynamics.

154 *2.2 Experimental conditions*

155 Particles used in our experiments include 4 grain-size classes of Glass Beads (GB), i.e. with
156 diameter < 32 μm, between 32-45 μm, between 45-63 μm, and between 63-90 μm as well as 6
157 grain-size classes of Andesitic, Rhyolitic, and Basaltic Volcanic Ash (Andes-VA; Rhyol-VA;
158 Basalt-VA, respectively), i.e. with diameter < 32 μm, 32-45 μm, 45-63 μm, 63-90 μm, 90-125 μm,
159 and 125-180 μm (Table 1). An additional class was also considered, where we mixed all the
160 particles with diameter <125 μm (called <125 μm in Table 1) to study the effect of using a widely
161 polydisperse mixture. Populations of different particle size were obtained through mechanical

sieving at the University of Geneva and the above-mentioned grain-size classes have been named after the sieves used which follow the international standard classification ISO3310. Laser diffraction analyses carried out with the CILAS 1180 instrument on selected samples indicate a good sorting inside the considered ranges (Folk and Ward, 1957).

For the andesitic composition, we used samples of volcanic ash erupted during the 2010 eruption of Eyjafjallajökull volcano (Iceland). This eruption produced a continuous volcanic plume up to 10 km above sea level between 14 April and 21 May 2010 (Gudmundsson et al., 2012). Glass composition ranges from benmoreite to trachyte with a silica content between 56 and 68 wt% and a total alkali from 7.3 and 9.1wt% (Cioni et al., 2014). The ash considered in our experiments was sampled between 4 and 8 May 2010 (Bonadonna et al., 2011). For the rhyolitic composition, we used samples of volcanic ash erupted during the May 2008 eruption of Chaitén volcano (Chile) (Alfano et al., 2011; Alfano et al., 2012; Alfano et al., 2016). The bulk magma composition of the main phase of this eruption varies between 73.0 and 75.5 wt% of SiO_2 (Alfano et al., 2011). Finally, for the basaltic composition, we used samples of volcanic ash from the 1992 eruption of Cerro Negro (Nicaragua) that lasted for about 21 days and was associated with a volcanic plume up to about 7 km a.s.l. (e.g. Connor and Connor, 2006; Connor et al, 1993). The silica content varies between 48.64 and 52.15 wt% (Roggensack et al., 1997). The density of individual size classes is complex to determine; however, based on the detailed analysis of Eychenne and Le Pennec (2012), we can assume that the density of fine ash is close to their Dense Rock Equivalent (DRE) value. The mean DRE value (measured with a helium pycnometer) of Eyjafjallajökull, Chaitén and Cerro Negro ash is 2738 kg m^{-3} (Bonadonna et al. 2011), 2240 kg m^{-3} (Alfano et al. 2012) and 2988 kg m^{-3} (measured for this work), respectively.

Three concentrations were considered to generate fingers: *C1* = 3 g/l, *C2* = 4 g/l, *C3* = 5 g/l. The concentrations were chosen based on experimental constraints as reported in Manzella et al. (2015). In fact, both lower and higher concentrations are not detectable experimentally based on the grey scale measuring strategy. The particle volumetric concentration in the experiments is then in the

188 order of 10^{-9}, which, together with their capacity to reflect the laser light, confirms that the particles
189 used can be exploited as tracers in PIV analysis. This is also supported by the fact that they are
190 coupled with the fluid since both their Stokes and Sedimentation numbers are < 1 (i.e. they are in
191 the range of 10^{-4}-10^{-1} and 0.5-1, respectively) for the grain-size and particle composition analysed in
192 our experiments (Carazzo and Jellinek, 2012). A detailed list of experiments is reported in Table 1.
193 In unmixed conditions, different tests were carried using GB with different concentrations
194 (experiment 1-10), GB with different sizes (experiments 11-17), Andes-VA with different sizes
195 (experiments 18-24) and Andes-VA with different concentrations (experiments 25-26). Experiments
196 with mixed conditions were carried out only for GB and Andes-VA in the range between 45 and 63
197 μm (experiments 28-29) and for Andes-VA with diameter < 125 μm (experiments 27 and 30).
198 However, the experiment 27 did not provide a good PIV analysis and was not considered for further
199 analysis. Experiments were finally carried out for Rhyol-VA and Basalt-VA with all the grain size
200 classes considered (experiments 31-34) in unmixed conditions. Experiments with GB were repeated
201 up to three times to verify the repeatability of the measurements (e.g. experiments 12-13, 14-15 and
202 16-17), while experiments with volcanic ash were carried out only once because of the limited
203 amount of material available. It is worth mentioning that GB particles are more visible than
204 volcanic ash particles, reflecting the laser light more efficiently. Among volcanic particles, the
205 Andes-VA ones reflect the laser light best and therefore, once the effect of the composition has
206 been studied, these were preferred for tests with volcanic ash.

207 *2.3 Data analysis*

208 Images of 1624 x 1600 pixel sizes were taken at of 0.03 s time steps and each particle captured by
209 the camera that scattered the laser light was used for the PIV analysis with the Dynamic Studio
210 Software (DANTEC, http://www.cefd-imech.ac.vn/lab/3D_PIV/DynamicStudio%20Manual.pdf).
211 PIV technique is based on the fact that the image intensity field at each instant corresponds to the
212 position of the particles reflecting the laser light and it assumes that between two instants t and t +
213 Δt, i.e. two consecutive exposures to the laser light, all particles inside a previously defined

interrogation window have moved together with the fluid with the same displacement vector, ΔX. This interrogation area (IA) should be small enough to respect this assumption but large enough to contain at least 10 particles reflecting the laser light to evaluate the intensity field. On the other hand, the particle volume fraction should be smaller than 10^{-4}, so that they are easily visible and do not influence the fluid flow. For this reason, in order to find the most suitable interrogation window and thus increase the accuracy of the analysis, the Dynamic Studio Software uses an iterative process that reduces the size of the interrogation area progressively from 128x128 to 16x16 pixels. In this framework, using a spatially statistical cross-correlation function which relates the difference in image intensity between two instants, we are able to evaluate the displacement of the fluid and the velocity vector for each interrogation area (Raffel et al., 2007). In addition, the DANTEC software is also used to evaluate the finger speed (m/s) measuring the position of the finger front at different times, the divergence (s^{-1}) and the vorticity (s^{-1}) fields.

As also described in the Dynamic Studio software manual, the divergence of a 3D vector velocity field $\overline{U}$ is defined as:

$$div(\overline{U}) = \frac{\partial U}{\partial x} + \frac{\partial V}{\partial y} + \frac{\partial W}{\partial z}. \quad (1)$$

For planar data gradients, as the one analysed with PIV, it reduces to:

$$div(\overline{UV}) = \frac{\partial U}{\partial x} + \frac{\partial V}{\partial y} \quad (2)$$

with *x*, *y* and *z* indicating the axis associated with the length, height, and width in Figure 2. Non-zero divergence values could indicate local changes in density and, therefore, local changes of particles concentration or, when the fluid is incompressible, a non-negligible variation of the velocity in the z direction.

Vorticity is a vector quantity, which corresponds to the rotation of the fluids. For planar data gradient only the z-component of vorticity, ω_z, can be calculated:

$$\omega_z = \frac{\partial V}{\partial x} - \frac{\partial U}{\partial y}. \quad (3)$$

According to Tritton (1988), turbulent flows are characterised by non-zero, fluctuating vorticity. Even if the studied gravitational instabilities cannot be considered two-dimensional because they have a component in the out of plane direction (z = W in Figure 2), this component is significantly smaller than the longitudinal (x = L in Figure 2) and vertical (y = H in Figure 2) dimensions of the tank, i.e. a few millimetres versus tens of centimetres. In addition, a single finger is mostly axi-symmetrical with respect to the flow direction, so we can assume that what we observe in a single finger in the x-y plane would be similar to what we could observe in the y-z plane. As a result, we consider that the PIV two-dimensional analysis can globally capture the main flow dynamics involved in the gravitational instabilities.

3. RESULTS

Figure 3 shows selected images of the experiments using GB and Andes-VA particles between 32 and 45 μm and between 63 and 90 μm with C1 as concentration and in unmixed condition (experiments 11, 15, 20 and 22 in Table 1). Fingers are clearly visible a few seconds (> 3s) after the sheet is removed and are of approximately the same size in each experiment.

Our analysis shows that the descending fingers have an irregular shape during the formation stage, and descend with large caps at their tips (e.g. Figure 3). The number of fingers increases with particle concentration (Figure 4a), but does not depend on the particle size and composition (Figure 4b). The mean wavelength, given by L/n where L is the length of the box (30.3 cm) and n is the number of fingers, ranges between 2.2 and 2.9 cm. Finger speed has a poor dependence on the particle concentration in the range of concentration investigated here (Figure 4c) and increases with particle size (Figure 4d). The experimental error bars in Figures 4a and 4b was evaluated by the standard deviation obtained from the mean value of finger number in ten images taken 3 s after removing the sheet. The mean and standard deviation in Figures 4c and 4d are instead evaluated by the analysis of five fingers over the course of one whole experiment.

263 It is worth mentioning that particles greater than 125 μm did not generate fingers (experiment 18
264 in Table 1). The number of fingers also depends on the experimental conditions of the upper layer.
265 Figures 5a and 5b illustrate experiments with a "mixed" upper layer using GB and Andes-VA
266 between 45 and 63 μm (experiments 28 and 29 in Table 1) showing a higher number of fingers (2-3
267 fingers more for both cases) with respect to "unmixed" experiments. Finger speed, instead, is
268 independent of initial mixing.
269 We also analysed the evolution of finger dynamics with time. In general, the downward
270 movement of fingers was not steady and we observed similar oscillations to those reported in
271 Carazzo and Jellinek (2012). For the same class size, we found a general decrease of finger number
272 with time mainly at the interface due to the decrease of the particle concentration in the upper layer.
273 As an example, the experiment 11 in Table 1 (i.e. GB with size between 32-45 μm) shows 11 and 8
274 fingers, respectively, 5 and 30 s after the sheet was removed (Figures 6a and b). The speed of
275 fingers is about 4.5 ±1.1 mm/s and 2.4 ± 0.2 mm/s after about 7 and 20 s, respectively. This
276 behaviour was similar for different class sizes (e.g. Figures 6c and 6d). Figure 7 shows the variation
277 of the finger number with respect to time for GB between 45 and 63 μm (experiment 3). At the
278 beginning of the experiment, the number of fingers is 11±1 and after about 30 s the number of
279 fingers remains almost constant (between 7±1 and 6±1). A power law fits the evolution with time
280 well (R^2=0.88; Figure 7). We found that the finger speed was 4.6 ± 1.1, 3.0 ± 1.0 and 2.4 ± 1.3
281 mm/s at 10 s, at 20 s and 30 s, respectively. The study of finger evolution with time was also carried
282 out for Andes-VA particles (experiments 19, 29, and 30) and for volcanic ash with a wide range of
283 size (< 125 μm) showing similar trends. As an example, Figure 8 shows the experiment 24 in Table
284 1 carried out with Andes-VA. At the beginning of the experiment (< 10 s), fingers contain particles
285 with the widest size range. In fact, even though particle size cannot be quantitatively assessed with
286 PIV, a qualitative assessment can be made based on backscattering because larger particles show a
287 smaller backscattering of the laser light and are less visible in the images retrieved by the camera

than smaller particles. In agreement with our previous observations, this experiment also shows how both the number and speed of fingers decrease with time. In particular, we observe 12 and 11 fingers after 5 and 10 s and 9 and 8 fingers after 15 sec and 20 s, respectively. The associated speed is 7.9 ± 1.2, 6.1 ± 1.0, 4.6 ± 1.7 and 4.3 ± 0.8 mm/s after 5, 10, 15 and 20 s, respectively.

Finally, we investigated the divergence and vorticity fields for GB and Andes-VA with different particle size and, in general, we found that divergence was zero everywhere except at the interface and inside the fingers. Figure 9 shows how the highest variation of the relative values of divergence and vorticity are concentrated in the fingers, where we also notice an increase of the brightness coming from the laser reflection of the particles (Figure 9a). An increase in brightness is hence associated with an increasing number of reflecting particles. As aforementioned, a non-zero divergence for PIV planar data could be associated with a significant velocity component along the out of plane direction (width in Figure 2), which cannot be excluded considering the 3D nature of fingers. However, the occurrence of the highest variations in divergence, even if small, combined with an increase of brightness within the fingers (Figures 9a and 9b), could suggest a temporary and localized variation in particle concentration. By contrast, a fluctuation of vorticity values in the *x-y* plane can be associated with a turbulence motion regardless of the 3D nature of the fingers. We can then infer that gravitational instabilities could be likely associated with an increase of concentration and turbulence with respect to initial conditions.

4. DISCUSSION

Our experiments confirm previous findings that gravitational instabilities have a marked effect on the sedimentation of volcanic ash (e.g. Carazzo and Jellinek, 2012; Manzella et al., 2015) and the analysis of these instabilities provide new insights into the effect of particle concentration, size and composition and into the evolution of fingers with time. Based on the analysis of divergence and vorticity, the formation of gravitational instabilities also has implications on particle aggregation.

313 Results show how the number of fingers depends largely on particle concentration in the upper
314 layer, as already concluded by Hoyal et al. (1999), while finger speed mostly depends on particle
315 size. Even though basaltic particles were more difficult to analyze than silicic particles due to their
316 dark colour that does not reflect the laser light well, particle composition seems to play a negligible
317 role on finger dynamics (e.g. Figure 4).

318 We have also shown how the number of fingers decreases with a drop in particle concentration
319 in the upper layer of the tank. Hence, there must be a critical value of particle concentration below
320 which fingers cannot form. In this sense, our experimental observations suggest that only volcanic
321 clouds characterized by a relatively high mass load of particles, and, therefore, volcanic eruptions
322 associated with a large Mass Eruption Rate (MER), are likely to form gravitational instabilities. As
323 an example, gravitational instabilities were clearly observed during the 23rd November 2013
324 explosive event of Etna volcano (Italy) that was characterized by a MER of about 10^5 kg/s
325 (Andronico et al., 2015) (see Figure 1a). The eruptive plume of the 4th May 2010 Eyjafjallajökull
326 eruption (Iceland) (Manzella et al., 2015) and of the 17th June 1996 eruption of Ruapehu volcano
327 (New Zealand) (Bonadonna et al., 2005), which generated well-developed gravitational instabilities,
328 were also characterized by a MER of about 10^5 kg/s (e.g. Degruyter and Bonadonna, 2013; Ripepe
329 et al., 2011; Bonadonna et al., 2005) (see Figures 1b and 1c). Gravitational instabilities were also
330 observed at the bottom of volcanic clouds associated with the thermal plumes of the August-
331 October 1997 Vulcanian explosions of Montserrat volcano, which injected an average of about 10^8-
332 10^9 kg of tephra into the atmosphere in just a few seconds (Bonadonna et al., 2002) (Figure 1d). By
333 contrast, gravitational instabilities were not observed during the 2011 and 2012 explosive events of
334 Etna volcano that were characterized by a lower MER (~10^4 kg/s) (Andronico et al., 2014).

335 Another fundamental condition for the formation of gravitational instabilities in volcanic clouds
336 is the presence of fine ash. Indeed, gravitational instabilities only formed in our experiments in
337 association with the sedimentation of particles <125 μm. Our results match those reported by Carey
338 (2007), although he used a different set-up and different concentration, but similar particle

composition (i.e. 1991 Pinatubo dacitic tephra) and fluid (i.e. water). In addition, both sets of experiments were performed in water, and, therefore, the critical cut-off size of 125 μm could be even smaller in air (Carazzo and Jellinek, 2012). All previously mentioned eruptions (i.e. Etna 23 November 2013, Eyjafjallajökull 2010, Montserrat 1997 and Ruapehu 1996) were characterized by the presence of particles < 125 μm, i.e. ~6wt% for Ruapehu 1996, ~40wt% for Eyjafjallajökull 2010 and ~50-80wt% for the August-October 1997 Vulcanian explosions of Montserrat (Bonadonna et al., 2002; Bonadonna and Houghton 2005; Bonadonna et al., 2011). In addition, volcanic lightning that is typically associated with particle-laden jet and abundance of fine particles (Cimarelli et al., 2013), was observed during the 23 November 2013 Etna eruption.

Theory reported in Manzella et al. (2015) shows how an increase in particle concentration in the upper layer would increase g', and, therefore, the finger speed. In fact, finger velocity is equal to: $v_f = g'^{\frac{2}{5}}(v_p \frac{1}{4}\pi\delta^2)^{1/5}$, where v_p is the particle settling velocity, δ is the Particle Boundary Layer (PBL) thickness, g' is the reduced gravity of the PBL given by $g' = g\frac{\rho_{PBL}-\rho_a}{\rho_a}$, where g is the gravity and ρ_{PBL} and ρ_a are the density of PBL and of the atmosphere, respectively. As a result, the higher the particle concentration in volcanic plumes, the higher the finger speed. Although we investigated a small range, a slight increase of the finger speed with concentration is also confirmed by our experiments and by theory (e.g. Hoyal et al., 1999). This aspect should however be explored further by enlarging the concentration range. Moreover, the theory of Hoyal et al. (1999) can explain the observed increase of particle speed with particle size and the negligible effect of particle composition on finger dynamics. First, the larger the particle size, the larger the particle velocity v_p, and, therefore, the finger velocity v_f. Second, the main difference among the particle composition is the variation in density that, however, is negligible for particles < 125 μm (e.g. Bonadonna and Phillips, 2003; Eychenne and Le Pennec, 2012). In fact, the difference in DRE values is only between 2240 kg/m^3 for Chaitén rhyolitic ash and 2988 kg/m^3 for Cerro Negro basaltic ash. Furthermore, volcanic clouds represent a polydisperse mixture containing a wide range of particle

sizes even at medial-distal locations. Based on our results and theory, we expect that i) the number of fingers decreases with the distance from the vent and ii) the finger speed decreases with the distance from the vent for a combined effect of the reduction of both volcanic ash concentration and particle size in the upper layer.

Aggregation of ash particles into clusters with a higher terminal fall velocity leads to a reduction of the atmospheric lifetime (e.g. Brown et al., 2012; Costa et al., 2006; Durant, 2015). It has already been suggested that aggregation could be enhanced inside the fingers due to the high particle concentration (e.g. Carazzo and Jellinek, 2012). Our analysis of divergence and vorticity provides additional evidence that indicates the potential role of gravitational instabilities in forming particle aggregates. Fluctuations of divergence and vorticity inside the fingers could represent an increase of particle concentration and turbulence with respect to the surrounding regions, which increases the probability of collisions, and, therefore, promotes aggregation. Nonetheless, the formation of ash clusters within volcanic plumes and clouds and the sedimentation of single ash clusters independently of gravitational instabilities cannot be excluded, in particular when the cluster settling velocity is higher than the finger settling velocity (e.g. Manzella et al., 2015).

Finally, our results clearly show that the highest values of finger number and finger speed are associated with their initial formation and both decrease with time. This could be related to the decrease of particle concentration in the upper layer, which in our experiment progressively decreases with time. However, during an eruption, volcanic plumes are continuously fed at the eruptive vent and the decrease in finger number and speed could only occur at the end of the explosive activity. This also supports the idea that particle aggregation may be more efficient at the beginning of finger formation when the concentration is the highest.

5. CONCLUSIONS

A comprehensive physical characterization of the sedimentation processes occurring in volcanic plumes and clouds relies on a better understanding of the gravitational instabilities. We carried out

experiments using a Plexiglas tank of 50 cm x 30.3 cm x 7.5 cm equipped with a horizontal removable plastic pet sheet to separate the two layers. The upper layer was made up of water and particles, while the lower layer was a solution of water and sugar that was initially denser than the upper layer. After removing the horizontal plastic pet sheet, particles were illuminated with a laser and filmed with a HD camera and analysed by PIV. Our experimental investigations provide new insights into the mechanisms characterizing finger formation and finger dynamics. In particular:

1) Number of fingers and finger speed increase with particle concentration in the upper layer; this is in agreement with previous experimental observations (e.g., Carazzo and Jellinek, 2012; Manzella et al., 2015) and supports field observations, where fingers have been observed only in volcanic plumes with relatively high MER (i.e. MER$\geq 10^5$ kg/s);
2) Gravitational instabilities were observed only with particles <125 μm; this also concurs with previous experimental observations (i.e. Carey 2007; Carazzo and Jellinek, 2012) and confirms the idea that a relative abundance of fine ash is necessary to generate fingers. However, the size cut-off in air could be smaller due to different buoyancy;
3) Number of fingers and finger speed are independent of particle composition, suggesting that finger formation can occur independently of magma composition;
4) The relation between gravitational instabilities and particle aggregation was explored based on the analysis of divergence and vorticity inside the fingers. These values suggest heterogeneity in particle concentration and an increase in turbulent motion that need further exploration with experiments including the analysis of the 3D component. Given that a high concentration of particles <125 μm and turbulence are both factors promoting aggregation, we can conclude that particle aggregation could easily occur both at the base of the cloud where fingers form and inside fingers.

Acknowledgments

The authors are grateful to M. Prestifilippo and E. Rossi for the useful discussions, to L. Pioli, and J. Ruch for their help during the experiments at the Geneva laboratory and to F. Arlaud for technical support. The work was funded by the ESF Research Networking Programmes, Reference N°4257 MeMoVolc, by the project 'From observations to experiments: Describing and characterizing gravitational instabilities of volcanic plumes'. The contribution of C. Bonadonna was supported by the Swiss National Science Foundation project No 200021_156255. We thank James White (Executive Editor), Joe Dufek (associate Editor), David Jessop and one anonymous reviewer for their constructive comments that greatly improved the manuscript.

Figures and Table Captions

Figure 1. Gravitational instabilities associated with:

a) 23 November 2013 lava fountain of Etna volcano, Italy (photo by http://www.tboeckel.de/EFSF/efsf_etna/Etna2013/Etna_11_13/volcano_etna_11_2013_e.htm); b) Eyjafjallajökull plume on 4 May 2010, Iceland (photo by C. Bonadonna); c) 17 June 1996 eruption of Ruapehu volcano, New Zealand (photo from http://www.natgeocreative.com/photography/1302290); d) Vulcanian explosion in September 1997, Montserrat (photo adjusted from Bonadonna et al. (2002)).

Figure 2. Experimental set-up comprising a Plexiglas tank of 30.3 cm x 50 cm x 7.5 cm (*x* corresponding to the length (L) direction, *y* to the height (H), *z* to the width (W)), a removable pet sheet, a laser and a HD camera. Particles, HD Camera, and laser instrument are not to scale. The stirrer used in our mixed experiments is shown in Figure DR4 of the repository material of Manzella et al. (2015).

Figure 3. Images of experiments with: a) GB with diameter between 32-45 μm (experiment 11 in Table 1); b) GB with diameter between 63-90 μm (experiment 15 in Table 1); c) Andes-VA with diameter between 32-45 μm (experiment 22 in Table 1); and d) Andes-VA with diameter between 63-90 μm (experiment 20 in Table 1). Images (26 cm x 16.5 cm) are taken about 10 seconds after removing the horizontal pet sheet separating the two fluids in unmixed conditions.

Figure 4. Plots showing the number of fingers with respect to: a) particle concentration in the upper layer (g/l) for GB and Andes-VA and b) particle size (μm) for GB, Andes-VA, Rhyol-VA and Basalt-VA; and the speed of fingers with respect to: c) particle concentration in the upper layer (g/l) for GB, Andes-VA, and Theory (Hoyal et al., 1999) and d) particle size for GB and Andes-VA (μm) (experiments 19 to 26 and 31 to 43 in Table 1).

Figure 5. Images (26 cm x 16.5 cm) showing the number of fingers for the experiments with a mixed upper layer using a) GB between 45 and 63 μm (experiment 28 in Table 1) and b) Andes-VA between 45 and 63 μm (experiment 29 in Table 1).

Figure 6. Images (26 cm x 16.5 cm) of experiments with GB of diameter between 32-45 μm (experiment 11 in Table 1) taken a) 5 s and b) 30 s and of diameter between 45-63 μm (experiment 3 in Table 1) taken c) 5 s and d) 30 s after removing the horizontal pet sheet. Arrows indicate observed fingers.

Figure 7. Plot showing the evolution of the finger number with time for GB between 45-63 μm (experiment 3 in Table 1).

Figure 8. Images (26 cm x 16.5 cm) of experiment 24 in Table 1 that includes Andes-VA with a wide range of particle sizes (< 125 μm) imaged about a) 5 s, b) 10 s, c) 15 s, and d) 20 s after removing the horizontal pet sheet.

Figure 9. Image of the experiment 7 (Table 1) for GB between 45-63 μm a) after 15 s the finger formation; b) divergence (s^{-1}) and c) vorticity (s^{-1}) fields and d) divergence and vorticity values measured along the orange line across the finger in c).

Table 1. Summary of experiments: experiment number; particle composition including glass beads (GB), andesitic volcanic ash (Andes-VA), rhyolitic volcanic ash (Rhyol-VA), and basaltic volcanic ash (Basalt-VA); particle size (S) in μm; Concentration in g/l; the upper layer was both quiescent (i.e. unmixed experiments, or continually mixed using a rotary stirrer (i.e. mixed experiments) described in Manzella et al. (2015).

References

Adrian RJ (1991) Particle-imaging techniques for experimental fluid mechanics. Annu. Rev. Fluid Mech. 23:261–304

Adrian RJ (1995) Limiting resolution of particle image velocimetry for turbulent flow. Advances in Turbulence Research Pohang Korea 1-19 Postech

Adrian RJ (2005) 20 years of particle image velocimetry. Exp Fluids 39:159–69

475 Alexander D (2013) Volcanic ash in the atmosphere and risks for civil aviation: a study in European
476 crisis management. Int. J. Disaster Risk Sci. 4: 9–19
477 Alfano F, Bonadonna C, Volentik ACM, Connor CB, Watt SFL, Pyle DM, Connor LJ (2011)
478 Tephra stratigraphy and eruptive volume of the May, 2008, Chaiten eruption, Chile. Bull
479 Volcanol 73 (5): 613–630
480 Alfano F, Bonadonna C, Gurioli, L (2012) Insights into eruption dynamics from textural analysis:
481 the case of the May, 2008, Chaitén eruption. Bull Volcanol doi:10.1007/s00445-012-0648-3
482 Alfano F, Bonadonna C, Watt S, Connor C, Volentik A, Pyle DM (2016) Reconstruction of total
483 grain size distribution of the climactic phase of a long-lasting eruption: the example of the 2008–
484 2013 Chaitén eruption, Bull Volcanol, 78:46, doi:10.1007/s00445-016-1040-5
485 Andronico D, Scollo S, Lo Castro MD, Cristaldi A (2014) Representivity of incompletely sampled
486 fall deposits in estimating eruption source parameters: a test using the 12–13 January 2011 lava
487 fountain deposit from Mt. Etna volcano, Italy. Bull Volcanol (2014) 76:861 doi:10.1007/s00445-
488 014-0861-3
489 Andronico D, Scollo S, Cristaldi A (2015) Unexpected hazards from tephra fallouts at Mt Etna: The
490 23 November 2013 lava fountain. Journal Volcanololgy Geothermal Research 204: 118-125
491 Blong, R., 2000, Assessment of volcanic risk, in Sigur, H., et al., eds., Encyclopedia of Volcanoes:
492 San Diego, Academic Press, p. 1215–1225. Bonadonna C, Macedonio G, Sparks RSJ (2002)
493 Numerical modelling of tephra fallout associated with dome collapses and Vulcanian explosions:
494 application to hazard assessment on Montserrat. Geological Society London Memoir 2002
495 Bonadonna C, Mayberry GC, Calder ES, Sparks RSJ, Choux C, Jackson P, Lejeune AM, Loughlin
496 SC, Norton GE, Rose WI, Ryan G, Young SR (2002) Tephra fallout in the eruption of Soufrière
497 Hills Volcano, Montserrat. In: Druitt TH Kokelaar BP (eds) The eruption of Soufrière Hills
498 Volcano, Montserrat, from 1995 to 1999. Geological Society, London, Memoir, v. 21, p. 483-
499 516, doi:10.1144/GSL.MEM.2002.021.01.22

500 Bonadonna C, Phillips JC (2003) Sedimentation from strong volcanic plumes. J Geophys Res,
501 108(B7): 2340 doi:10.1029/2002JB002034
502 Bonadonna C, Houghton BF (2005) Total grain-size distribution and volume of tephra-fall deposits.
503 Bull Volcanol 67:441-456
504 Bonadonna C, Phillips JC, Houghton BF (2005a) Modeling tephra fall from a Ruapehu weak plume
505 eruption. J Geophys Res 110(B08209) doi:10.1029/2004JB003515
506 Bonadonna C, Connor CB, Houghton B.F, Connor L, Byrne M, Laing A, Hincks TK (2005b)
507 Probabilistic modeling of tephra dispersion: Hazard assessment of a multi-phase rhyolitic
508 eruption at Tarawera, New Zealand. J Geophys Res 110:B03203 doi:10.1029/ 2003JB002896
509 Bonadonna C, Genco R, Gouhier M, Pistolesi M, Cioni R, Alfano F, Hoskuldsson A, Ripepe M
510 (2011) Tephra sedimentation during the 2010 Eyjafjallajökull eruption (Iceland) from deposit,
511 radar, and satellite observations. J Geophys Res, 116, B12202, doi:10.1029/2011JB008462
512 Bonadonna C, Folch A, Loughlin S, Puempel H (2012) Future developments in modelling and
513 monitoring of volcanic ash clouds: outcomes from the first IAVCEI-WMO workshop on Ash
514 Dispersal Forecast and Civil Aviation. Bull Volcanol 74: 1-10
515 Brown RJ, Bonadonna C, Durant AJ (2012) A review of volcanic ash aggregation. Phys Chem
516 Earth A/B/C 45-46: 65-78
517 Carazzo G, Jellinek AM (2012) A new view of the dynamics, stability and longevity of volcanic
518 clouds. Earth Planet Sci Lett 325-326: 39–51
519 Carazzo G, Jellinek AM (2013) Particle sedimentation and diffusive convection in volcanic ash-
520 clouds. Journal Geophysical Research 118:1420-1437
521 Cardoso SSS, Zarrebini M (2001) Convection driven by particle settling surrounding a turbulent
522 plume. Chemical Engineering Science 56:3365–3375
523 Carey SN (1997) Influence of convective sedimentation on the formation of widespread tephra fall
524 layers in the deep sea. Geology 25: 839-842

525 Carey SN, Sigursson H (1982) Influence of particle aggregation on deposition of distal tephra from
526 the May 18, 1980, eruption of Mount St. Helens volcano. Journ Geophys Res 87: 7061-7072
527 Chojnicki KN, Clarke AB, Adrian RJ, Phillips JC (2014) The flow structure of jets from transient
528 sources and implications for modeling short-duration explosive volcanic eruptions. Geochem
529 Geophys Geosyst 15, 4831–4845
530 Chojnicki KN, Clarke AB, Phillips JC, Adrian RJ (2015a) Rise dynamics of unsteady laboratory
531 jets with implications for volcanic plumes' Earth and Planetary Science Letters 412: 186-196
532 Chojnicki KN, Clarke AB, Phillips JC, Adrian RJ (2015b) The evolution of volcanic plume
533 morphology in short-lived eruptions Geology 43:707-710
534 Cioni R, Pistolesi M, Bertagnini A, Bonadonna C, Hoskuldsson A, Scateni B (2014) Insights into
535 the dynamics and evolution of the 2010 Eyjafjallajökull summit eruption (Iceland) provided by
536 volcanic ash textures. Earth and Planetary Science Letters 394: 111-123
537 Cimarelli C, Alatorre-Ibargüengoitia MA, Kuppers U, Scheu B, Dingwell DB (2013) Experimental
538 generation of volcanic lightning. Geology doi:10.1130/G34802.1
539 Connor LJ, Connor CB (2006) Inversion is the key to dispersion: understanding eruption dynamics
540 by inverting tephra fallout. In:Mader H, Coles SG, Connor CB, Connor LJ (eds) Statistics in
541 volcanology. Geological Society, London, pp 231–242
542 Connor CB, Powell L, Strauch W, Navarro M, Urbina O, Rose WI (1993) The 1992 eruption of
543 Cerro Negro, Nicaragua: An example of Plinian-style activity at a small basaltic cinder cone.
544 Eos, Transactions of the American Geophysical Union, 74: 640
545 Costa A, Macedonio G, Folch A (2006) A three dimensional Eulerian model for transport and
546 deposition of volcanic ashes. Earth Planet. Sci. Lett. 241: 634–647
547 Degruyter W, Bonadonna C (2013) Impact of wind on the condition for column collapse of volcanic
548 plumes. 377: 218-226

549 Durant AJ; Rose WI (2009) Hydrometeor-enhanced tephra sedimentation: Constraints from the 18
550 May 1980 eruption of Mount St. Helens. Journal Geophysical Research 114: doi:
551 10.1029/2008JB005756
552 Durant (2015) Toward a realistic formulation of fine-ash lifetime in volcanic clouds Geology. 43:
553 271-272
554 Eychenne J, Le Pennec JL (2012) Sigmoidal particle density distribution in a subplinian scoria fall
555 deposit. Bull Volc 74:2243-2249
556 Elissondo M, Baumann V, Bonadonna C, Pistolesi M, Cioni R, Bertagnini A, Biass S, Herrero JC,
557 and Gonzalez R (2016) Chronology and impact of the 2011 Cordón Caulle eruption, Chile. Nat.
558 Hazards Earth Syst. Sci., 16: 675–704
559 Folch (2012) A review of tephra transport and dispersal models: Evolution, current status, and
560 future perspectives. Journal of Volcanology and Geothermal Research 235-236: 96-115
561 Folk RL and Ward WC (1957) Brazos River bar: a study in the significance of grain size
562 parameters. Journal of Sedimentary Petrology, 27: 3–26.
563 Grant I (1997) Particle image velocimetry: A review. Proceeding of the Institution of mechanical
564 engineers part C- Journal of Mechanical Engineering Science, 211, 1: 55-76
565 Gudmundsson MT, Thordarson T, Hoskuldsson A, Larsen G, Bjornsson H, Prata FJ, Oddsson B,
566 Magnusson E, Hognadottir T, Petersen GN, Hayward CL, Stevenson JA, Jonsdottir I (2012) Ash
567 generation and distribution from the April-May 2010 eruption of Eyjafjallajokull, Iceland.
568 Scientific Reports, 2: doi: 10.1038/srep00572
569 Hoyal D, Bursik MI, Atkinson JF (1999) Settling-driven convection: A mechanism of
570 sedimentation from stratified fluids. J Geophys Res 104 (C4): 7953-7966
571 Manzella I, Bonadonna C, Phillips JC, Monnard H. (2015) The role of gravitational instabilities in
572 deposition of volcanic ash. Geology 43: 211-214
573 Miller TP, Casadevall TJ (2000) Volcanic Ash Hazards to Aviation. Encyclopedia of Volcanoes.
574 Sigurdsson, H., Academic Press, San Diego, CA

575 Oxford Economics (2010) The Economic Impacts of Air Travel Restrictions Due to Volcanic Ash
576 Report for Airbus, available at: http://controverses.mines-
577 paristech.fr/public/promo10/promo10_G11/data/documents/Volcanic-Update.pdf
578 Raffel M,Willert C,Wereley S, Kompenhans J. (2007) Particle Image Velocimetry: A Practical
579 Guide. New York: Springer
580 Ripepe M, Bonadonna C, Folch A, Delle Donne D, Lacanna G, Marchetti E, Hoskuldsson A,
581 Hoeskuldsson A (2011) Ash-plume dynamics and eruption source parameters by infrasound and
582 thermal imagery: The 2010 Eyjafjallajokull eruption, Earth and Planetary Science Letters 366:
583 112-121
584 Roggensack K, Hervig R L, McKnight SB, Williams SN (1997) Explosive Basaltic Volcanism from
585 Cerro Negro Volcano: Influence of Volatiles on Eruptive Style. Science 277: 1639-1641
586 Saffaraval F, Solovitz SA, Ogden DE, Mastin LG (2012) Impact of reduced near-field entrainment
587 of overpressured volcanic jets on plume development, Journal of Geophysical Research 117:
588 B05209, doi:10.1029/2011JB008862
589 Sammons P, McGuire B, Edwards S (2010) Volcanic hazard from Iceland – analysis and
590 implications of the Eyjafjallajokull eruption, UCL Institute for Risk and Disaster Reduction
591 report, London, available at: https://www.ucl.ac.uk/rdr/documents/docs-publications-
592 folder/icelandreport
593 Schultz DM, Kanak KM, Straka JM, Trapp RJ, Gordon BA, Zrnic DS, Bryan GH, Durant AJ,
594 Garrett TJ, Klein PM, Lilly DK (2006) The mysteries of mammatus clouds: Observations and
595 formation mechanisms. Journal of the Atmospheric Sciences 63: 2409–2435
596 Scollo S, Tarantola S, Bonadonna C, Coltelli M, Saltelli A (2008) Sensitivity analysis and
597 uncertainty estimation for tephra dispersal models. Journal of Geophysical Research-Solid Earth,
598 113:B06202, doi:10.1029/2006JB004864

599 Scollo S, Folch A, Coltelli M, Realmuto VJ (2010) Three-dimensional volcanic aerosol dispersal: a
600 comparison between MISR data and numerical simulations. Journal of Geophysical Research-
601 Atmospheres 115:doi: 10.1029/2009JD013162
602 Telling J, Dufek J (2012) An experimental evaluation of ash aggregation in explosive volcanic
603 eruptions. Journal of Volcanology and Geothermal Research 209: 1-8
604 Tritton D J (1988) Physical Fluid Dynamics, Oxford University Press, Oxford
605 Turner JS (1979) Buoyancy effects in fluids: Cambridge, Cambridge University Press
606 Wilson T, Stewart C, Bickerton H, Baxter P, Outes V, Villarosa G, Rovere E. (2013) Impacts of the
607 June 2011 Puyehue- Cordón Caulle volcanic complex eruption on urban infrastructure,
608 agriculture and public health. GNS Science, New Zealand, GNS Science Report 2012/20: 88

Figure 1

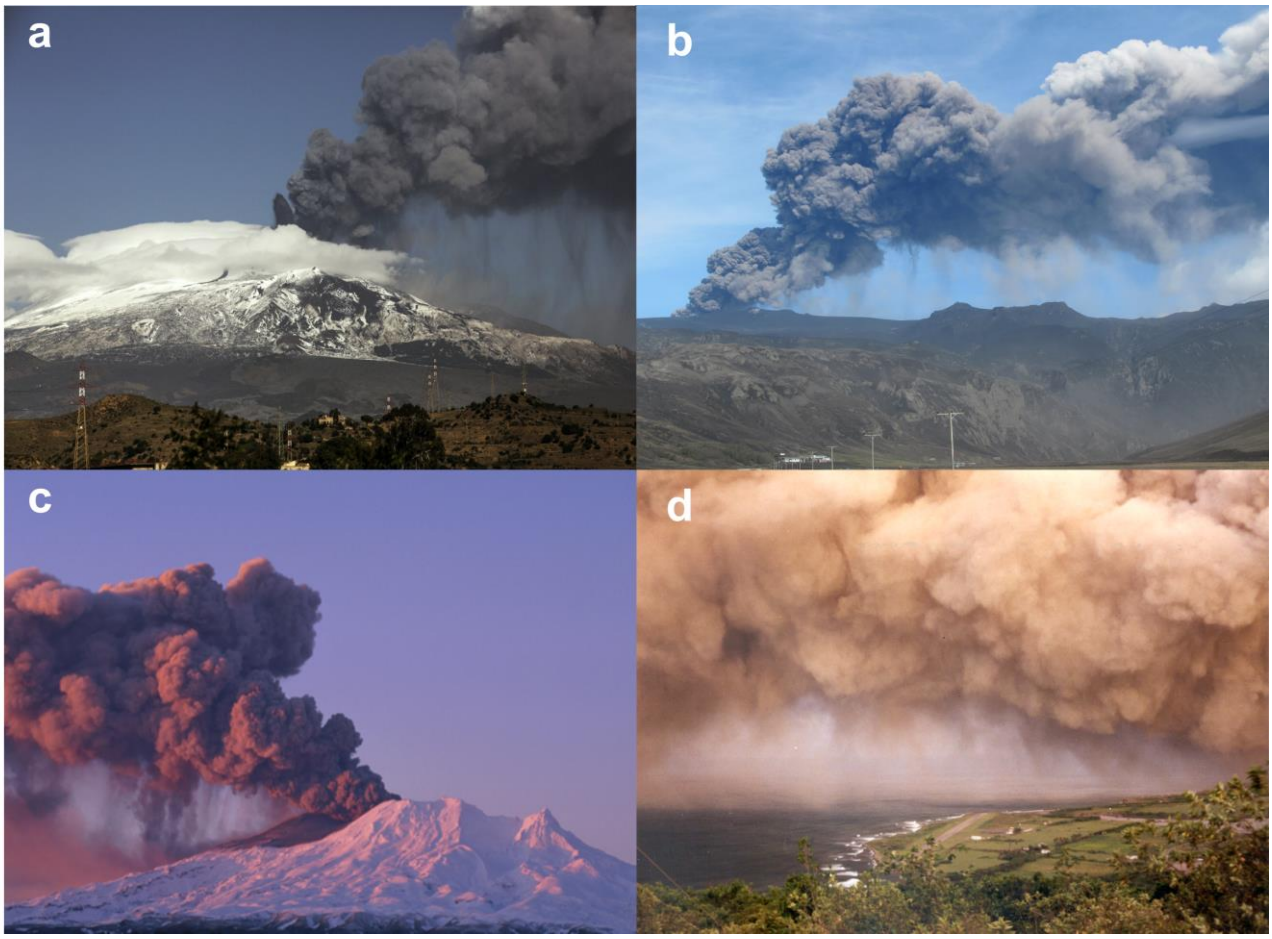

Figure 2

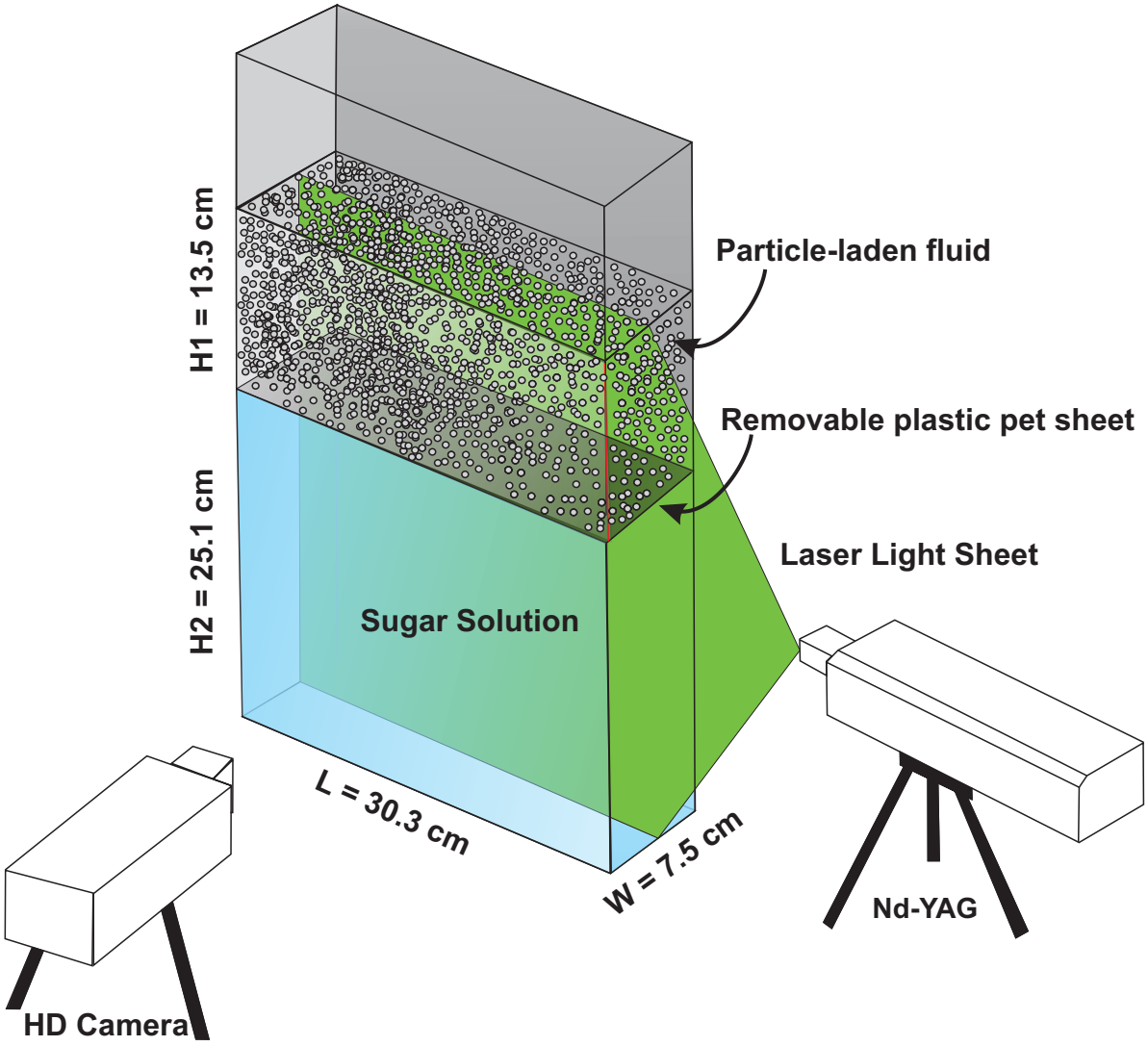
H1 = 13.5 cm
H2 = 25.1 cm
Particle-laden fluid
Removable plastic pet sheet
Laser Light Sheet
Sugar Solution
L = 30.3 cm
W = 7.5 cm
Nd-YAG
HD Camera

Figure 3

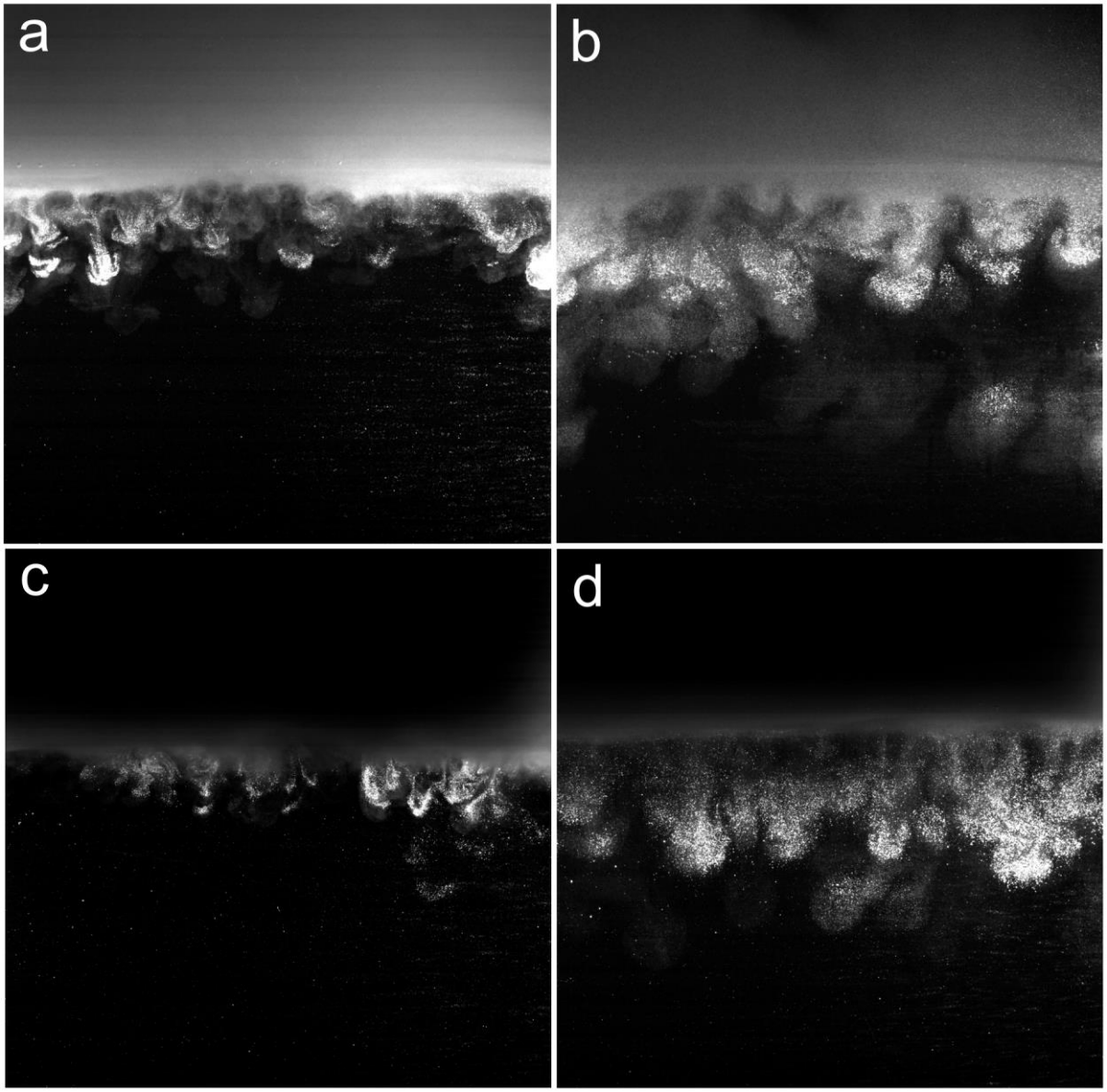

Figure 4

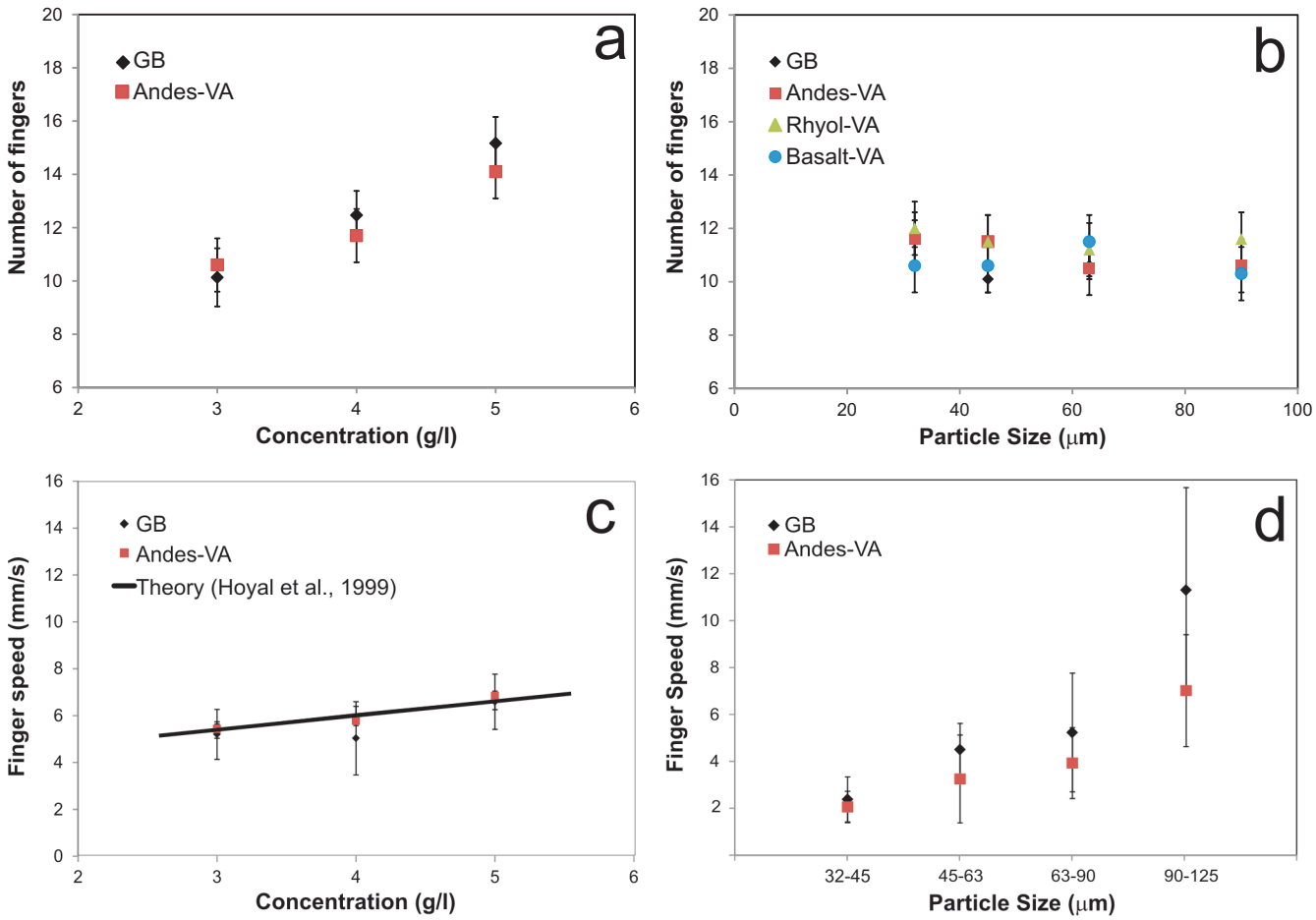
a
GB
Andes-VA
Number of fingers
Concentration (g/l)
b
GB
Andes-VA
Rhyol-VA
Basalt-VA
Number of fingers
Particle Size (μm)
c
GB
Andes-VA
Theory (Hoyal et al., 1999)
Finger speed (mm/s)
Concentration (g/l)
d
GB
Andes-VA
Finger Speed (mm/s)
32-45
45-63
63-90
90-125
Particle Size (μm)

Figure 5

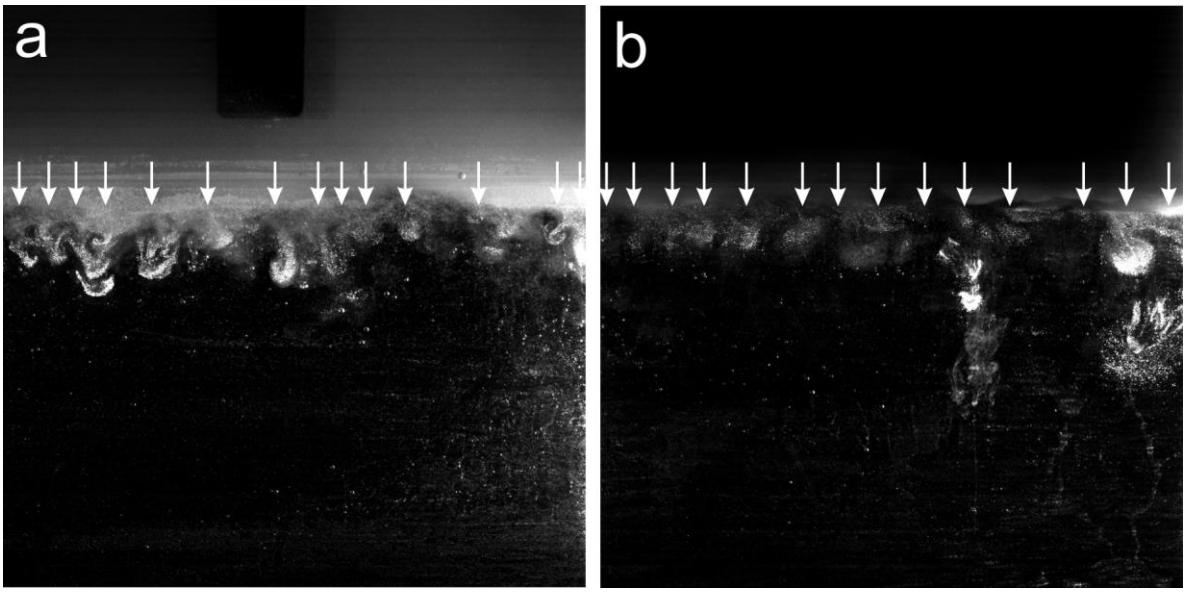

Figure 6

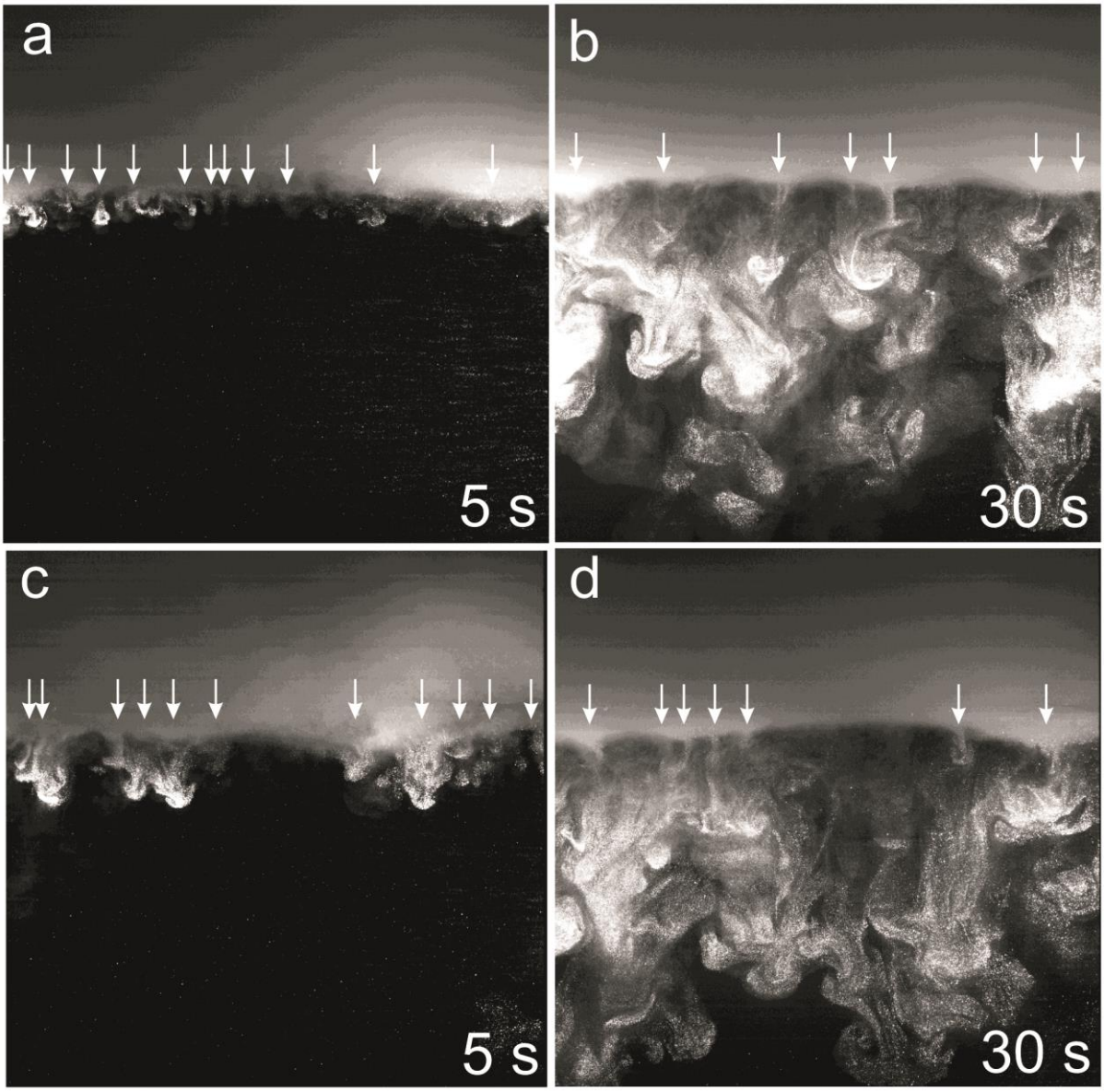

Figure 7

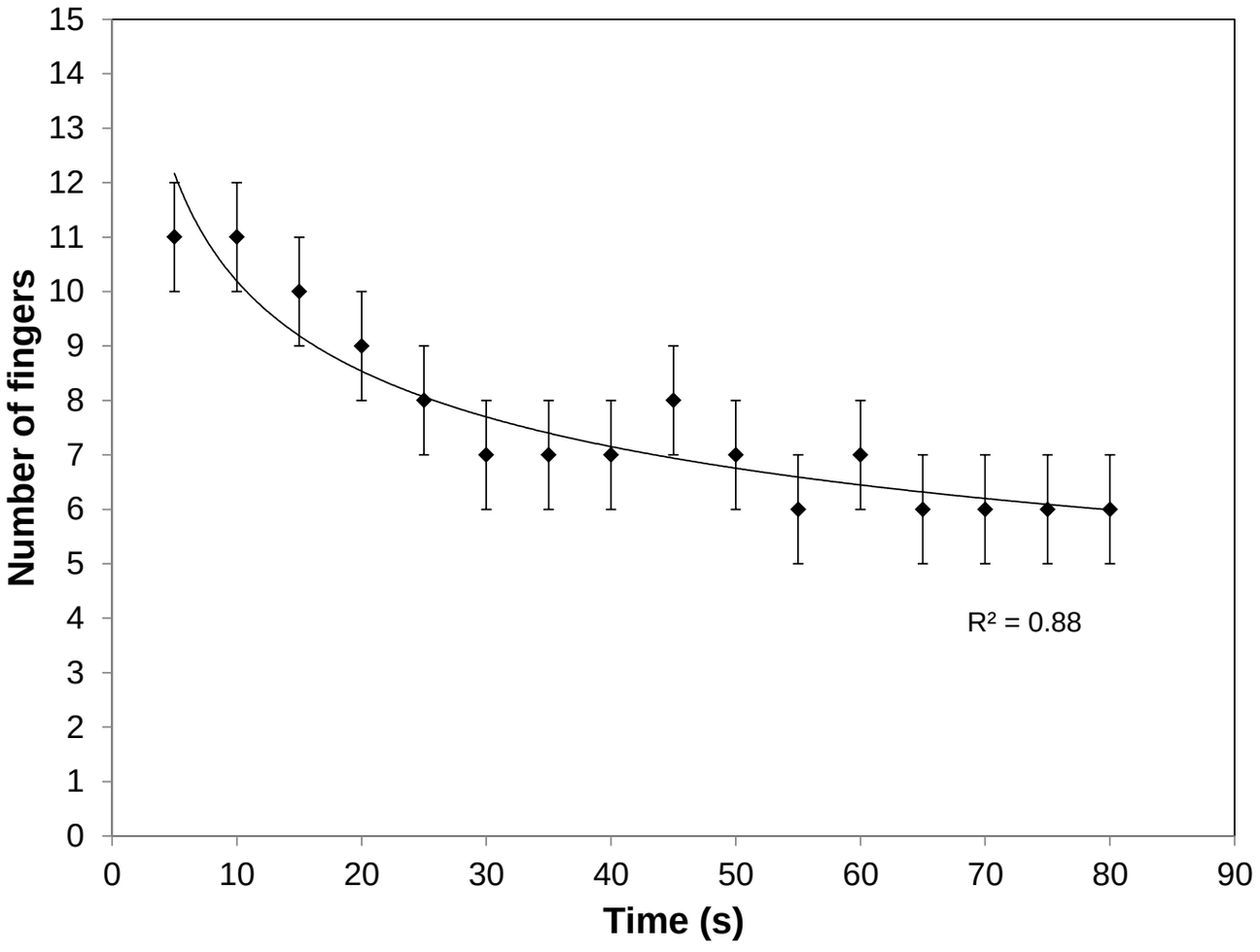
Number of fingers
Time (s)
R² = 0.88
0
1
2
3
4
5
6
7
8
9
10
11
12
13
14
15
0
10
20
30
40
50
60
70
80
90

Figure 8

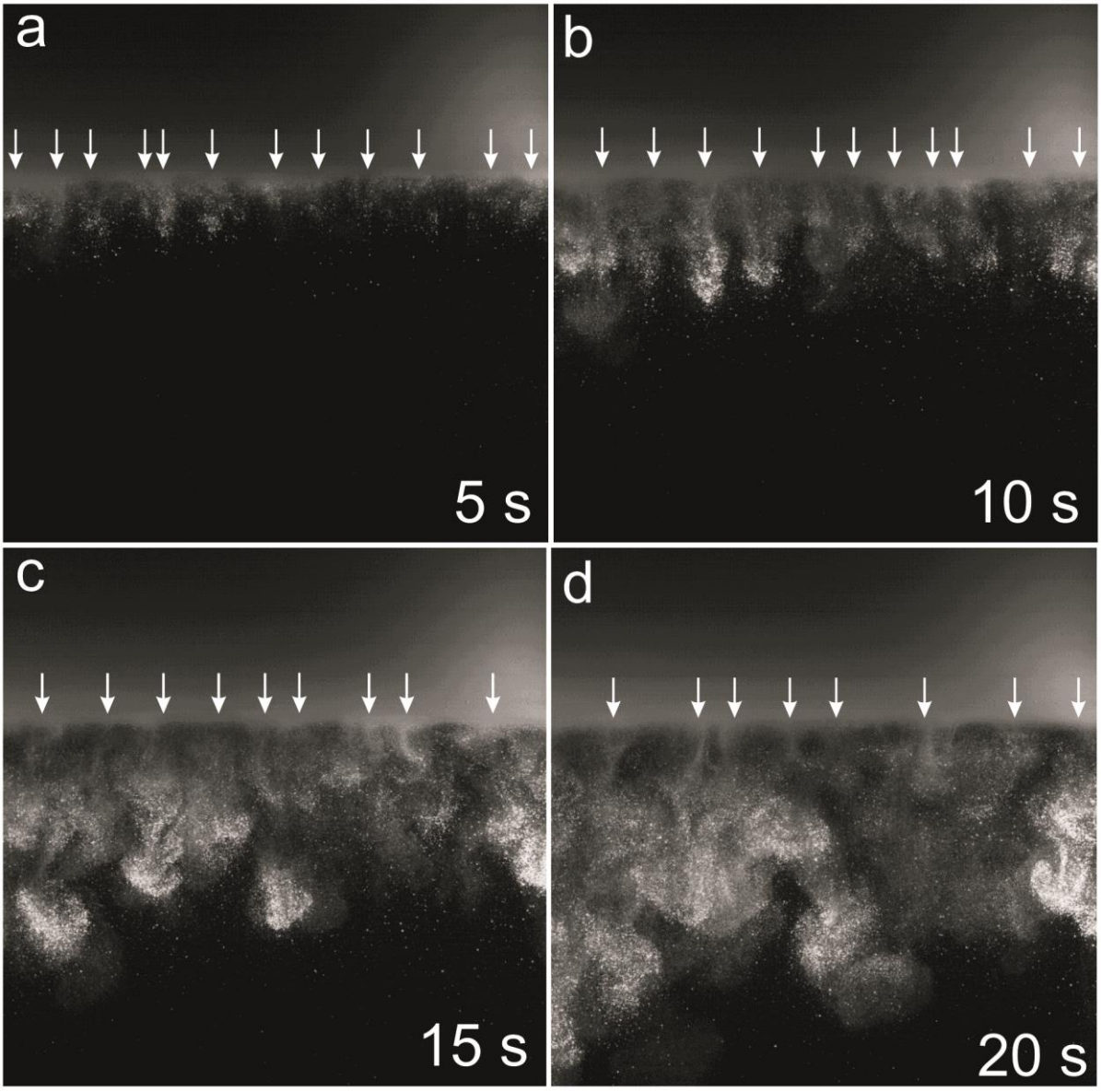

Figure 9

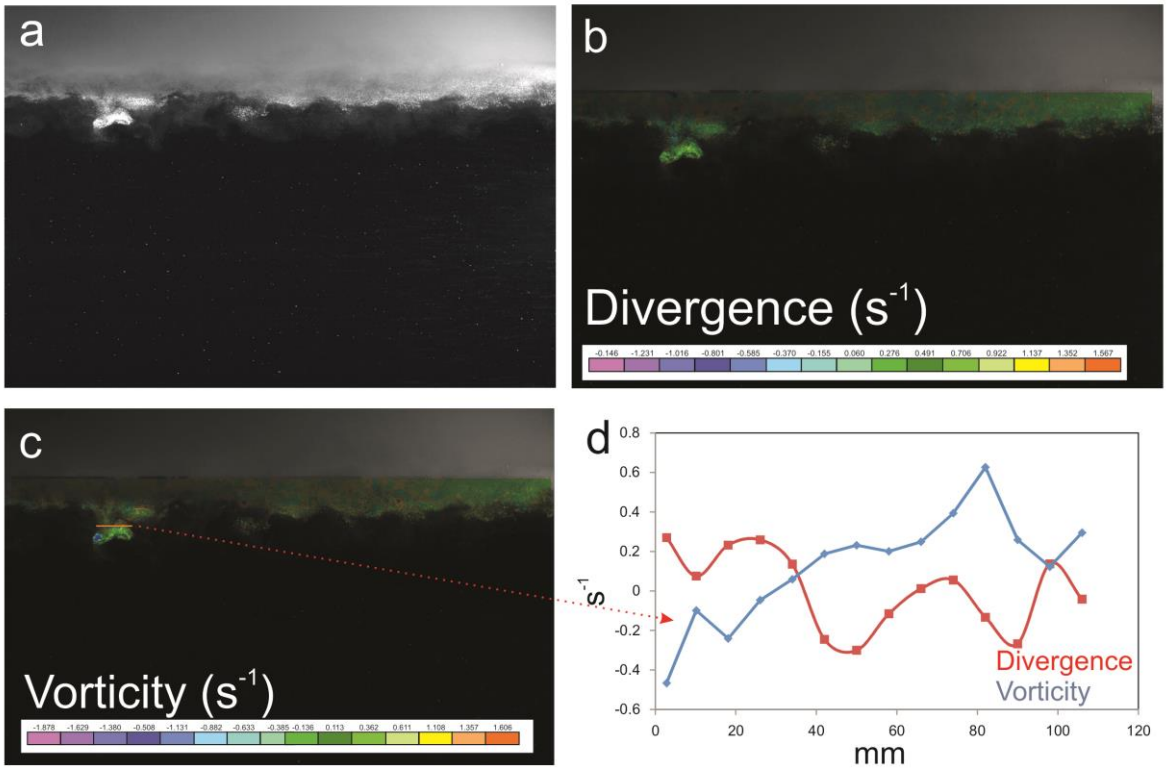
a
b
Divergence (s-1)
-0.146 -1.231 -1.016 -0.801 -0.585 -0.370 -0.155 0.060 0.276 0.491 0.706 0.922 1.137 1.352 1.567
c
Vorticity (s-1)
-1.878 -1.629 -1.380 -0.508 -1.131 -0.882 -0.633 -0.385 -0.136 0.113 0.362 0.611 1.108 1.357 1.606
d
0.8
0.6
0.4
0.2
0
-0.2
-0.4
-0.6
s-1
0 20 40 60 80 100 120
mm
Divergence
Vorticity

Table 1

Experiment number	Particle composition	Particle size (μm)	Concentration (g/l)	Experiment conditions
1	GB	45-63	3	Unmixed
2	GB	45-63	3	Unmixed
3	GB	45-63	3	Unmixed
4	GB	45-63	4	Unmixed
5	GB	45-63	4	Unmixed
6	GB	45-63	4	Unmixed
7	GB	45-63	4	Unmixed
8	GB	45-63	5	Unmixed
9	GB	45-63	5	Unmixed
10	GB	45-63	5	Unmixed
11	GB	32-45	3	Unmixed
12	GB	32-45	3	Unmixed
13	GB	32-45	3	Unmixed
14	GB	63-90	3	Unmixed
15	GB	63-90	3	Unmixed
16	GB	<32	3	Unmixed
17	GB	<32	3	Unmixed
18	Andes-VA	125-180	3	Unmixed
19	Andes-VA	90-125	3	Unmixed
20	Andes-VA	63-90	3	Unmixed
21	Andes-VA	45-63	3	Unmixed
22	Andes-VA	32-45	3	Unmixed
23	Andes-VA	<32	3	Unmixed
24	Andes-VA	<125	3	Unmixed
25	Andes-VA	63-90	4	Unmixed
26	Andes-VA	63-90	5	Unmixed
27	Andes-VA	<125	3	Mixed
28	GB	45-63	3	Mixed
29	Andes-VA	45-63	3	Mixed
30	Andes-VA	<125	3	Mixed
31	Rhyol-VA	<32	3	Unmixed
32	Rhyol-VA	32-45	3	Unmixed
33	Rhyol-VA	45-63	3	Unmixed
34	Rhyol-VA	63-90	3	Unmixed
35	Rhyol-VA	90-125	3	Unmixed
36	Rhyol-VA	<125	3	Unmixed
37	Basalt-VA	<32	3	Unmixed
38	Basalt-VA	32-45	3	Unmixed
39	Basalt-VA	45-63	3	Unmixed
40	Basalt-VA	63-90	3	Unmixed
41	Basalt-VA	90-125	3	Unmixed
42	Basalt-VA	<125	3	Unmixed
43	Basalt-VA	<32	3	Unmixed